Estimating the Meridional Extent of Adiabatic Mixing in the Stratosphere using Age-of-Air

Aman Gupta[1,2,3], Marianna Linz[4], Jezabel Curbelo[5], Olivier Pauluis[2], Edwin P. Gerber[2], Douglas E. Kinnison[6]

[1]Meteorological Institute Munich, Ludwig-Maximilian University, Munich, BY, Germany
[2]Center for Atmosphere-Ocean Science, Courant Institute of Mathematical Sciences, New York, New York, USA
[3]Department of Earth System Science, Stanford University, Stanford, CA, USA
[4]Department of Earth and Planetary Sciences and School of Engineering and Applied Sciences, Harvard University, Cambridge, MA, USA
[5]Departament de Matemàtiques, Universitat Politècnica de Catalunya, Barcelona, Spain
[6]Atmospheric Chemistry Observations and Modeling Laboratory, National Center for Atmospheric Research, Boulder, CO, USA

Key Points:

- The isentropic formulation of the leaky pipe stratospheric transport model (Linz et al., 2021) is used to estimate midlatitude mixing fluxes
- A new metric, which quantifies the meridional range of air parcels being mixed across transport barriers, is proposed to estimate mixing
- The deep tropical stratosphere is remarkably isolated and mixes with the extratropics only in the uppermost stratosphere

Corresponding author: Aman Gupta, `Aman.Gupta@lmu.de`

Abstract

Wave-induced adiabatic mixing in the winter midlatitudes is one of the key processes impacting stratospheric transport. Understanding its strength and structure is vital to understanding the distribution of trace gases and their modulation under a changing climate. age-of-air is often used to understand stratospheric transport, and this study proposes refinements to the vertical age gradient theory of Linz et al. (2021). The theory assumes exchange of air between a well-mixed tropics and a well-mixed extratropics, separated by a transport barrier, quantifying the adiabatic mixing flux across the interface using age-based measures. These assumptions are re-evaluated and a refined framework that includes the effects of meridional tracer gradients is established to quantify the mixing flux. This is achieved, in part, by computing a circulation streamfunction in age-potential temperature coordinates to generate a complete distribution of parcel ages being mixed in the midlatitudes. The streamfunction quantifies the "true" age of parcels mixed between the tropics and the extratropics. Applying the revised theory to an idealized and a comprehensive climate model reveals that ignoring the meridional gradients in age leads to an underestimation of the wave-driven mixing flux. Stronger, and qualitatively similar fluxes are obtained in both models, especially in the lower-to-middle stratosphere. While the meridional span of adiabatic mixing in the two models exhibits some differences, they show that the deep tropical pipe, i.e. latitudes equatorward of 15° barely mix with older midlatitude air. The novel age-potential temperature circulation can be used to quantify additional aspects of stratospheric transport.

1 Introduction

The large-scale stratospheric circulation, known as the Brewer-Dobson Circulation (BDC), plays a primary role in transporting long-lived trace gases throughout the stratosphere, thereby determining their spatial distributions. The BDC brings tropospheric air up into the stratosphere through the tropical tropopause and transports the air vertically and poleward. The breaking of planetary waves in the upper stratosphere and synoptic waves in the lower stratosphere both drives this meridional circulation across isentropes (diabatic) and mixes air horizontally along isentropic surfaces (adiabatic). This adiabatic mixing moves tracers over large spatial scales and plays an important role in exchanging midlatitude air with tropical air (Plumb, 2002). From a Lagrangian perspective, an air parcel entering the stratosphere will experience both diabatic advection and

adiabatic mixing over the course of its time in the stratosphere (Hall & Plumb, 1994; Garny & Randel, 2016).

The trace gases we observe in the stratosphere tend to be those that are long-lived. On short timescales, these gases can be treated as passive tracers advected by the background flow. When the relative importance of the chemistry is small, the trace gas concentration is dominantly determined by transport. It has been found that isopleths (surfaces of constant mixing ratio) of different trace gases with varied chemistry have nearly identical shapes (Mahlman et al., 1986; Plumb & Ko, 1992). For instance, trace gases exhibit weak meridional gradients in the midlatitudes due to rapid horizontal mixing. In contrast, observations of trace gases reveal sharp local gradients in concentration in the subtropics and near the edge of the polar vortex, indicating existence of transport barriers (Neu et al., 2003; Shah et al., 2020).

Understanding the mixing across these transport barriers is important for climate and climate change: the distribution of trace gases determines their associated radiative forcing, and mixing plays a key role in transporting ozone-depleting substances into the polar vortex where they act as catalysts for ozone depletion (Lee et al., 2001). Intensification in isentropic mixing has been known to increase the residence time of trace gases in the stratosphere (Neu & Plumb, 1999; Garny et al., 2014), increasing their likelihood of participating in ozone-destroying chemical reactions. Isentropic mixing is strongly influenced by the mean flow and the wave-propagation conditions, especially in the winter stratosphere (Charney & Drazin, 1961; Holton et al., 1995). Moreover, changes in mixing can further project on to changes in the BDC strength itself, as enhanced mixing can potentially increase the diabatic upwelling of mass and trace gases into the stratosphere. Therefore, these non-linear changes will collectively play a key role in determining transport trends throughout the stratosphere in a changing climate (Ploeger et al., 2012, 2015; Abalos et al., 2016).

In order to understand short-term changes and long-term trends in isentropic mixing in the stratosphere, it is essential to first accurately estimate the wave-induced mixing fluxes. Several past studies have attempted to investigate the spatial structure of mixing through use of both dynamical and tracer-based metrics (Konopka et al., 2009; Abalos & de la Cámara, 2020). For instance, eddy diffusivity, which depends on the eddy flux of potential vorticity and vorticity gradients, has been used to quantify mixing ex-

clusively using dynamical quantities (Plumb & Mahlman, 1987; Schneider, 2004). This idea has also been extended to measure eddy diffusivity of a tracer by redefining the diffusivity in terms of eddy flux and meridional gradient of the trace gas (Nakamura, 2001). Many other studies have analyzed the seasonality and long-term trends in adiabatic mixing through use of effective diffusivity (Allen & Nakamura, 2001; Shuckburgh et al., 2001; Chen & Plumb, 2014; Abalos et al., 2016), or other methods including Lyapunov diffusivity (Shuckburgh et al., 2009) and Lagrangian diffusivity (Curbelo et al., 2021).

While each method offers physical insights, each has its own set of limitations. For instance, studies using effective diffusivity frequently employ a coordinate transformation and work in the "equivalent latitude" space, instead of regular latitudes. This makes it non-trivial to connect changes and trends in mixing in the specialized coordinates to changes in true mixing; especially as the equivalent latitude is itself defined in terms of tracer contours which may substantially change over time. Moreover, computing effective diffusivity requires computing multiple spatial derivatives and integrals, which is not always readily possible for limited observational data.

An alternative approach is to formulate the transport-dynamics coupling using theoretical or simple models of stratospheric transport (Plumb, 1996; Neu & Plumb, 1999; Ray et al., 2016). In order to mathematically model trace gas transport, these models study advection of an idealized tracer called "age-of-air" (Hall & Plumb, 1994; Waugh & Hall, 2002). Age-of-air quantifies how long an air parcel has been in the stratosphere and can be defined analytically. It is an effective tool to both quantify the transport timescales of trace gases in the stratosphere, and to study the transport of observed trace gases (Hall & Plumb, 1994). This is because, like many trace gases, one formulation of the age-of-air tracer has no spatial sources/sinks in the stratosphere (Boering et al., 1996); only a linear trend at the domain boundary. Thus, there exists a compact relation between the idealized tracer age-of-air and other chemically active trace gases (Plumb & Ko, 1992; Plumb, 2007). In fact, it is possible to directly estimate age-of-air from satellite observations of various atmospheric trace gases (Waugh & Hall, 2002; Linz et al., 2017), and age can also be readily computed in climate models either through time-lag analysis or through use of an idealized "clock" tracer (Hall et al., 1999; Garcia et al., 2011; Gerber, 2012). A similar approach has been used by several past studies focused on using the age-of-air distribution to infer dynamical properties of the stratosphere (Ray et al., 2010; Garny et al., 2014; Linz et al., 2016, 2021).

Of particular interest to this study are the recent works of Linz et al. (2016) and Linz et al. (2021), which proposed a theoretical framework using age-of-air to estimate the magnitude and vertical structure of both the diabatic circulation strength and the midlatitude mixing flux in the stratosphere. They used age-of-air to assess transport in the stratosphere and connect it to the large-scale circulation. Simply put, Linz et al. (2016) re-formulated the tropical "leaky pipe" model of Neu and Plumb (1999) in isentropic coordinates and established an inverse relationship between the diabatic circulation strength and the difference between tropical and extratropical age-of-air. Further, Linz et al. (2021) proposed a vertical age gradient theory which connects the net aging of air in the tropical "pipe" to the combined effects of aging due to the slow diabatic advection within the tropics and to the adiabatic mixing of air between the tropical pipe and the extratropics.

Both the age-of-air and the transport diagnostics proposed in the studies can be computed using satellite observations and/or climate models through straightforward integration. Therefore, this approach can be potentially used to directly and quantitatively connect observations to theory and models. This enables inference of dynamical properties of the stratosphere that are difficult to directly measure using satellite measurements of trace gases, as explore by Linz et al. (2017).

In this study, we propose a framework to improve the mixing flux estimates obtained by Linz et al. (2021). To motivate this analysis, estimates of mixing rates derived by applying their theory for two different models, one idealized (GFDL-FV3) and one comprehensive (WACCM), are shown in Figure 1(a). Qualitatively similar mixing structures are obtained for the two models in that the mixing maximizes in the lower stratosphere: near 400 K for the idealized model (red) and near 500 K for the comprehensive model (gray). Above this level, the mixing rapidly decreases to near-zero in the middle stratosphere, before exhibiting a small increase again in the upper stratosphere. The level of maximum mixing differs for the two models on account of a lower tropopause in the idealized model (Linz et al., 2021).

The models, however, show some key differences in the vertical mixing structure as well, observed in both the mixing rates (Figure 1(a)) and mixing efficiency (Figure 1(b)). Mixing efficiency, a dimensionless quantity, is a ratio of the mixing flux to the net poleward mass flux and captures the vertical mixing structure in the stratosphere. Apart

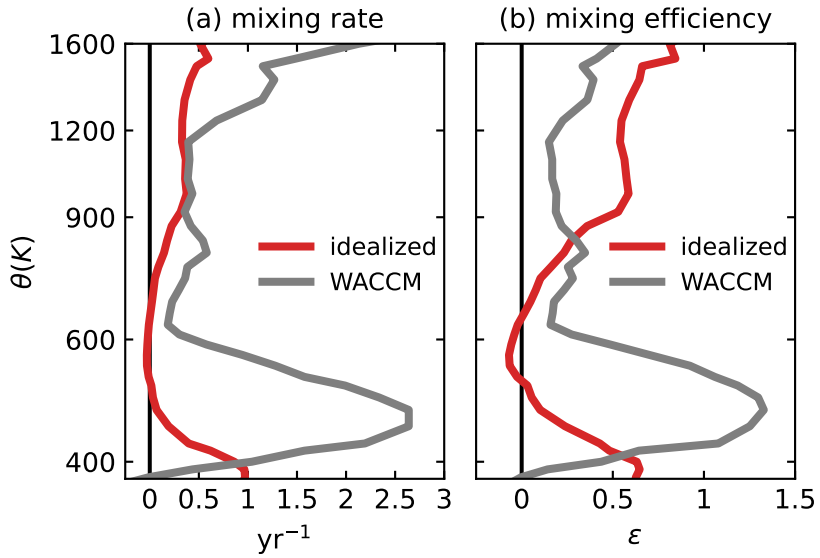

Figure 1. (a) Derived mixing rate of air (in yr^{-1}) from the winter midlatitudes stratosphere into the tropical stratosphere inferred from (red) an idealized finite volume dynamical core (FV3) with a perpetual January climatology and (grey) a comprehensive model (WACCM) for NDJFM months. Linz et al. (2021) define the mixing rate as the ratio of the estimated mixing flux (units kg/K/s) and the horizontally integrated isentropic density (units kg/K). (b) Mixing efficiency (a proxy for mixing) derived from the inferred mixing rates in (a). Mixing efficiency (ϵ) is a dimensionless quantity and is defined as the ratio of the net mixing flux and the net poleward flux. The net poleward flux, μ_{net}, is defined as the vertical convergence of the net diabatic flux in the tropical pipe. For exact definitions see Equation (17) of Linz et al. (2021).

from the differences in mixing peaks between the idealized (400 K) and the comprehensive model (500 K), the idealized model exhibits a significantly weaker mixing over the 400-600 K interval. These differences cannot be attributed to differences in the tropopause height alone. In fact, the mixing is weak to the extent that the estimated mixing flux and efficiency, which should be non-negative by definition, assumes non-sensical negative values around 600 K in the idealized model. Similar mixing differences and negative mixing estimates were also found among the models in the annual mean calculations of Linz et al. (2021) (their Figure 5). More pronounced negative mixing fluxes were obtained by Gupta et al. (2021), who used the theory to compare mixing fluxes among a broad range of idealized models.

Rectifying the false negative flux estimates, reconciling the difference in mixing between the two models, and ultimately obtaining more accurate mixing fluxes, are the goals of this study. We show that "negative" mixing appears due to an incorrect assumption of a perfectly-mixed tropics and midlatitudes. The Linz et al. (2021) theory assumes fast horizontal mixing within each of the tropical and extratropical "pipes", so neglecting tracer gradients within each region. This effectively implies the deep tropics are mixing just as much as with the extratropics as air at the edge of the pipe, and that the polar air is mixing just as much with the tropics as midlatitude air. This incorrent assumption leads to a potential underestimation of the mixing fluxes across the mixing barrier. In reality, adiabatic mixing is more localized to the winter midlatitudes with only occasional intrusions into the polar vortex or subtropics.

It is possible to get a more accurate estimate of mixing fluxes by accounting for subtropical gradients. We refine the theory of Linz et al. (2021) accordingly to account for the sensitivity of the mixing estimates to strong subtropical gradients. These refinements enable us to improve the mixing flux estimates without compromising the simplicity of their model. Both the original mixing theory and our refinement to correct for the strong meridional gradients within each "pipe" are discussed in Section 2. Section 3 presents the model setup for the idealized and comprehensive model assessed in this study. We apply the proposed theory and discuss our results in Section 4. Finally, we draw conclusions from the analysis and discuss potential avenues for further research in Section 5.

2 A refined theory to estimating the mixing flux

The isentropic formulation of Linz et al. (2016, 2021) begins with the horizontally integrated, mass-flux weighted ages Γ_u and Γ_d over respective regions of diabatic upwelling and diabatic downwelling respectively. They are defined as:

$$\Gamma_u(\theta) = \frac{\int_u \rho_\theta \dot{\theta} \Gamma dA}{\int_u \rho_\theta \dot{\theta} dA} \;\; ; \;\; \Gamma_d(\theta) = \frac{\int_d \rho_\theta \dot{\theta} \Gamma dA}{\int_d \rho_\theta \dot{\theta} dA} \tag{1}$$

where θ is the potential temperature, $\dot{\theta}$ is the diabatic velocity, $\rho_\theta = \frac{-1}{g} \left| \frac{d\theta}{dp} \right|$ is the isentropic density, Γ is the age-of-air, the integrand dA is the infinitesimal area element in the latitude-longitude space, p is the pressure, and the subscripts $\int_u$ and $\int_d$ respectively

denote selective integration over regions of diabatic upwelling ($\dot{\theta} > 0$) and diabatic downwelling ($\dot{\theta} < 0$).

Linz et al. (2021) showed that for a steady circulation, in the limit of no vertical diffusion and fast horizontal mixing, the vertical age gradient in the tropical pipe is the sum of aging due to vertical advection and aging due to adiabatic mixing. Mathematically, this is expressed as :

$$\underbrace{\frac{d\Gamma_u}{d\theta}}_{\text{T1 : vertical gradient}} = \underbrace{\frac{\sigma_u}{\mathcal{M}}}_{\text{T2 : advection}} + \underbrace{\mu_{mix}\frac{\Delta\Gamma}{\mathcal{M}}}_{\text{T3 : bulk mixing}} \tag{2}$$

where θ is the potential temperature, $\Delta\Gamma = \Gamma_d - \Gamma_u$ is the age difference between the extratropics and the tropics, $\mathcal{M}$ is the diabatic mass flux, σ_u (units of kg/K) is the isentropic density (ρ_θ) horizontally integrated over region of upwelling and μ_{mix} is the mass flux per Kelvin that mixes the midlatitude air with the tropical air. The advection term T2 captures the net aging of air as it is advected by the diabatic circulation up the tropical pipe: the mass of air per unit potential temperature (kg/K) divided by the flux of mass (kg/s)—literally, how long it takes the air to rise one unit of potential temperature. The bulk mixing term T3 captures the total aging of the tropical pipe by older air mixed in from the extratropics: $\Delta\Gamma$ quantifies how much older this extratropical air is relative to the tropics, and $\mu_{mix}/\mathcal{M}$ quantifies the relative contribution of this air per unit Kelvin.

All the terms in the mixing equation except μ_{mix} can be computed from the winds and age-of-air. Thus, the mixing flux μ_{mix} is estimated as a residual in Equation 2. For a more detailed discussion, see Section 3 of Linz et al. (2021) and Appendix A. As we will show, computing the mixing as a residual allows errors in other terms to corrupt the implied mixing flux.

2.1 Modification to the vertical age gradient equation

Both the original leaky pipe formulation (Neu & Plumb, 1999) and the isentropic formulation of Linz et al. (2021) assume fast horizontal mixing of trace gases within the upwelling and downwelling regions. With sufficiently fast mixing, the horizontal gradient of age-of-air within each region can be ignored, and thus the age of all parcels in each region can be simply assumed to be $\Gamma_u(\theta)$ and $\Gamma_d(\theta)$, the corresponding mass flux weighted age-of-air in the upwelling/downwelling regions. It follows that the entrainment flux trans-

ports parcels with a fixed age Γ_u across the barrier towards higher latitudes, and the mixing flux transports parcels with a fixed age Γ_d back to lower latitudes. The mixing term T3 in Equation 2 is therefore interpreted as the bulk mixing flux μ_{mix} which mixes the meridional age difference $\Delta\Gamma$ between the two regions.

The meridional profile of age-of-air estimated from observations and models, however, exhibits sharp tracer gradient around the sub-tropical barrier (Waugh & Hall, 2002). For instance, age at 50 hPa from the benchmark tests of Gupta et al. (2020) (shown in Figure 4(b) later) linearly increases from 3 Yr at the equator to 5.5 Yr around the sub-tropical barrier. Further poleward, in the surf-zone, the meridional gradient is much weaker on account of wave-induced mixing. Therefore, assuming a perfectly-mixed tropics leads to an overestimation of the actual age difference between air being mixed between the tropics and the extratropics. The midlatitude mixing, which is the main driver of horizontal churning of trace gases, does not generally extend all the way to the equatorial region. As will be shown in later sections, the deep tropics, especially in the middle and lower stratosphere, are fairly isolated from the wave-induced mixing fluxes that originate in the surf-zone. Consequently, assuming perfectly mixed tropics and extratropics leads to an underestimation of the midlatitude mixing flux μ_{mix} from Equation 2.

Consider perturbations $\delta\Gamma_u$ and $\delta\Gamma_d$ to the mean ages Γ_u and Γ_d respectively on a given isentrope, and assume that instead of air with the tropical mean age Γ_u mixing with air with the extratropical age Γ_d, slightly older air in the tropics with age $\Gamma_u+\delta\Gamma_u$ mixes with a slightly younger air from the extratropics with age $\Gamma_d-\delta\Gamma_d$. Physically, this captures the fact that the mixing is more localised around the turnaround latitude and does not span the entirety of the two regions. Re-deriving the mixing equation with this assumption yields the *revised mixing equation* :

$$\underbrace{\frac{d\Gamma_u}{d\theta}}_{\text{C1}} = \underbrace{\frac{\sigma_u}{\mathcal{M}}}_{\text{C2}} + \underbrace{\mu^T_{mix}\frac{\Delta\Gamma_{eff}}{\mathcal{M}}}_{\text{C3 : true mixing}} - \underbrace{\mu_{net}\frac{\delta\Gamma_u}{\mathcal{M}}}_{\text{C4 : enterainment freshening}} \tag{3}$$

where $\Delta\Gamma_{eff} = \Delta\Gamma-(\delta\Gamma_u+\delta\Gamma_d)$ is the effective age difference being mixed across the barrier, following the modification, and μ_{net} is the net poleward flux defined as the vertical diabatic flux convergence, i.e. $\mu_{net} = -\frac{\partial\mathcal{M}}{\partial\theta}$. Substituting $\delta\Gamma_u = \delta\Gamma_d = 0$ yields the original mixing equation of Linz et al. (2021). The detailed derivation is provided in the Appendix. The advective term C2 on the right is identical to T2 in Equation 2.

The total age difference $\Delta\Gamma$ in term T3 in Equation 2 is now replaced with the effective age difference $\Delta\Gamma_{eff}$ in the true mixing term C3 in Equation 3. The age perturbations $\delta\Gamma_u$ and $\delta\Gamma_d$ should be non-negative, so $\Delta\Gamma_{eff} \leq \Delta\Gamma$; the true age difference of the parcels mixed between the two regions is smaller than the age difference $\Delta\Gamma$. In later sections, it is shown that for the idealized dynamical core setup the perturbations $\delta\Gamma_u$ and $\delta\Gamma_d$ are indeed positive. This, however, cannot be said to be generally true for the comprehensive model WACCM due to complications in interpreting the annual cycle. An additional term C4 now appears in Equation 3: the air leaving the tropics is older than the mean age Γ_u and this term corrects the net poleward age transport. For non-negative perturbations, C4 should also be non-negative and provide a positive offset/correction to the mixing flux estimate from Equation 2. The updated C3 and new C4 terms provide a positive "correction" to yield the true mixing flux μ^T_{mix}.

In order to compute the true mixing flux using equation 3, an estimate of the perturbation ages $\delta\Gamma_u$ and $\delta\Gamma_d$ is needed. To compute these, we define a $\Gamma-\theta$ circulation distribution in the following subsection. The circulation distribution provides a comprehensive description of the age range of parcels being transported at a given latitude and isentropic height allowing us to estimate the perturbation ages $\delta\Gamma_u$ and $\delta\Gamma_d$. To differentiate between the mixing estimates obtained from Equation 2 and 3, we will hereafter refer to μ_{mix} estimated from Equation 2 as the "bulk mixing flux" and μ^T_{mix} estimated from Equation 3 as the "true mixing flux".

2.2 Computing $\delta\Gamma_u$ and $\delta\Gamma_d$ with diabatic circulation as a function of age

The schematic in Figure 2(a) provides an intuitive introduction to the Γ-θ circulation, showing the meridional wind (black) and age-of-air (color) on a fixed, arbitrarily chosen, 475 K ($\approx$ 70 hPa) isentropic surface as a function of latitude and longitude. Our goal is to switch from viewing this circulation in longitude to viewing this circulation in age: at 60°N, for instance, what is the age of mass moving poleward and equatorward? We see that the poleward advected air across this latitude is, on average, younger than the equatorward advected air. The Γ-θ circulation provides the entire distribution of this transport.

To compute the Γ-θ circulation, we first isolate a chosen isentropic surface with $\theta = \theta_0$. Further, we selectively consider only a chosen $\Gamma = \Gamma_0$ contour on this chosen isentrope. Finally, we compute the mean meridional mass transport exclusively associated with the chosen potential temperature and age-of-air level. This provides the net mass flux associated with the whole range of ages associated with the transported parcels on the selected θ_0-isentrope.

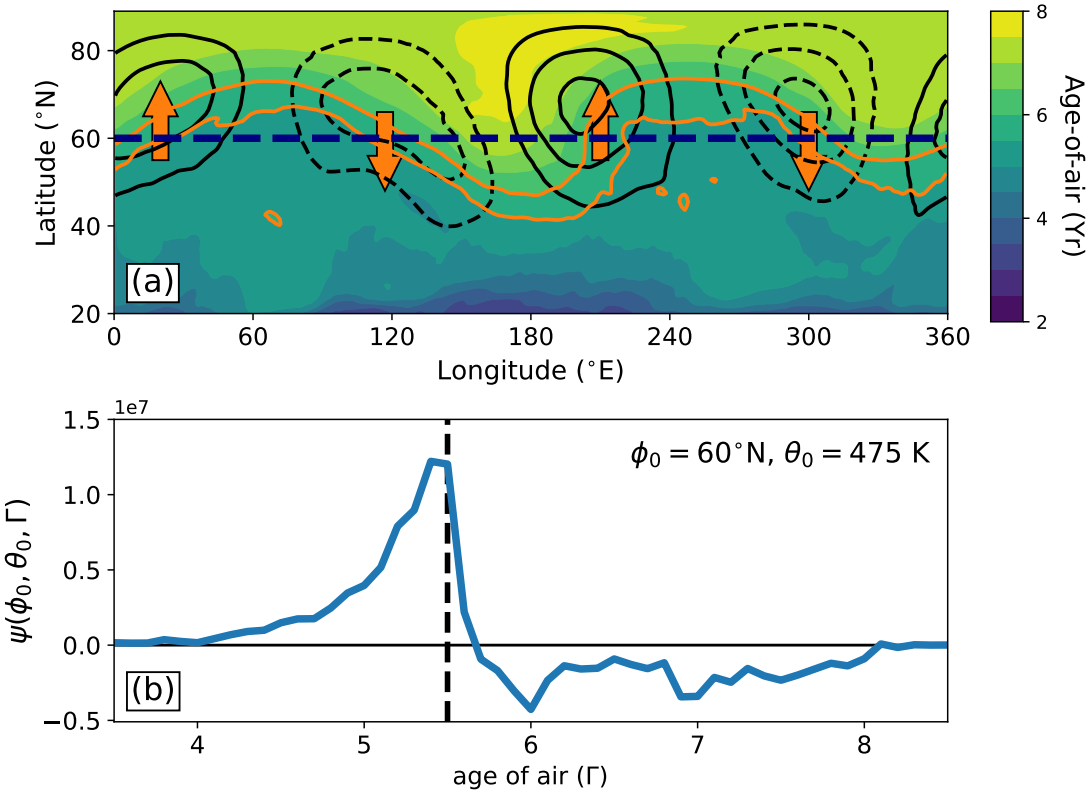

Figure 2. (a) A schematic providing physical intuition behind the mathematical formulation of the Γ-θ circulation defined in Equation 4. The solid and dashed curves show the positive and negative meridional velocity on the 475 K isentropic surface, as marked by the orange arrows. The colors show the contours of age-of-air which is transported by the meridional flow across a given latitude (dashed blue). The 5.5 yr age contour is highlighted with orange borders. (b) Γ-θ circulation at 60°N on the 475 K isentrope, as a function of age. The vertical bar in dashed black marks an age of 5.5 Yr corresponding to the orange contours in (a). The age Γ in the horizontal axis corresponds to the integrand Γ' in Equation 5.

The Dirac-delta formulation of the diabatic streamfunction developed by Pauluis et al. (2009), computes meridional mass transport in moist isentropic coordinates in the troposphere through selective binning of mass transport into potential temperature bins or levels. Pauluis et al. (2009) use the approach to estimate a joint distribution of mass transport as a function of both dry and moist potential temperature by using two Dirac-delta functions (see Equation (1) of Pauluis et al. (2009) for details). This study follows a similar approach to obtain the joint distribution of the meridional mass transport as a function of both potential temperature (θ) and age-of-air (Γ). Mathematically, this is akin to using two Dirac-delta functions, one for potential temperature and one for age in order to bin the meridional mass transport according to both the potential temperature and the mean age of the parcels being transported. The joint Γ-θ meridional mass transport distribution, ψ, can thus be expressed as :

$$\psi(\phi, \theta_0, \Gamma_0) = \frac{2\pi R \cos\phi}{g} \int_0^{2\pi} \int_0^{p_s} v\delta(\theta - \theta_0)\delta(\Gamma - \Gamma_0)\, dp d\lambda \tag{4}$$

where ϕ is the latitude, θ_0 and Γ_0 are the select potential temperature and age bins at which the circulation is sampled, v is the meridional velocity on model pressure levels, $\delta(\cdot)$ is the Dirac-delta function, p_s is the surface pressure, dp and $d\lambda$ represent vertical and zonal integration respectively, R is the radius of earth, and g is the acceleration due to gravity. To compute the zonal averages in the integral on isentropic surfaces, the isentropic binning technique introduced in Yamada and Pauluis (2015) was used, as it allows us to avoid direct computation of the isentropic density. For brevity, we hereafter refer to the quantity ψ as the Γ-θ *circulation*. In the northern hemisphere, positive values of ψ indicate poleward transport and negative values, equatorward transport. The signs are reversed for the southern hemisphere.

Revisiting Figure 2(a), for data originally on pressure levels, the Dirac-delta function $\delta(\theta - \theta_0)$ isolates the isentropic surface with $\theta = \theta_0$. Moreover, the Dirac-delta function $\delta(\Gamma - \Gamma_0)$ selectively considers only the $\Gamma = \Gamma_0$ contour on the chosen isentropic surface. For $\Gamma_0 = 5.5$ Yr, for instance, the two delta functions isolate the 5.5 Yr age contour, highlighted in orange, allowing us to compute the meridional mass transport along that contour. Finally, computing zonal mean along a latitude circle captures the net mean meridional circulation i.e., computing the net meridional transport only in the regions where the orange highlighted contours meets the (say) 60°N latitude circle (dashed blue). We compute the mass transport for a wide range of age levels from 0 to 15 Yr and show the mass streamfunction on 475 K and 60°N latitude in Figure 2(b).

For a given latitude circle, such as that shown in dashed blue, the net mass transport is distributed over a broad range of parcel ages. In this case, the circulation moves air parcels with age 4 Yr to 5.7 Yr poleward and air parcels with age 5.7 Yr to 8 Yr equatorward. The equatorward transport is spread over a much wider range at 60°N due to sharp tracer gradients poleward of 60°N on account of the polar vortex edge barrier. This can be clearly seen in Figure 2(a).

For a chosen latitude and potential temperature, ψ provides a distribution of meridional mass transport as a function of age. Therefore, it enables estimation of the complete range of ages of the parcels being transported by the meridional circulation of the stratosphere across a given latitude and on a given isentrope. This distribution is used to compute the true age being mixed around the transport barrier for a given isentrope, which in turn allows us to compute $\delta\Gamma_u$ and $\delta\Gamma_d$ needed for the refined theory in Equation 3.

To estimate the true age of the parcels being mixed between the upwelling and downwelling regions and hence $\delta\Gamma_u$ and $\delta\Gamma_u$, we calculate the Γ-θ circulation-weighted ages separately over the intervals of poleward vs equatorward mass transport at the turnaround latitude. This yields the *effective ages* $\Gamma_{u,eff}$ and $\Gamma_{d,eff}$ of the parcels being mixed across the turnaround latitude on this potential temperature surface. For latitudes in the northern hemisphere, the ages, expressed as a circulation-weighted average, can be expressed as:

$$\Gamma_{u,eff} = \frac{\int_{\psi>0} \psi\Gamma' \, d\Gamma'}{\int_{\psi>0} \psi \, d\Gamma'} \;\; ; \;\; \Gamma_{d,eff} = \frac{\int_{\psi<0} \psi\Gamma' \, d\Gamma'}{\int_{\psi<0} \psi \, d\Gamma'} \tag{5}$$

where the variable of integration, Γ', is the age-of-air, and the integration limit $\psi > 0$ means integration only over positive values of ψ. In our computations, Γ' ranges from 0 Yr to 15 Yr, which is the maximum age-of-air in our model runs. The difference between the effective and the mass flux-weighted ages is defined as the perturbation ages $\delta\Gamma_u$ and $\delta\Gamma_d$. More precisely, the Γ-θ circulation is used to estimate $\Gamma_{u,eff}$ and $\Gamma_{d,eff}$, and the perturbations are calculated as $\delta\Gamma_u = \Gamma_{u,eff} - \Gamma_u$ and $\delta\Gamma_d = \Gamma_d - \Gamma_{d,eff}$.

2.3 Eddy Diffusivity

The isentropic eddy diffusivity is an alternative method to assess the meridional profile of the mixing flux of age. Plumb and Mahlman (1987) and Schneider (2004) define eddy diffusivity as a diffusive parameterization of eddy fluxes in terms of zonal mean

quantities to obtain closure of the tracer continuity equation. Nakamura (1996), Shuckburgh et al. (2001), and Abalos et al. (2016) quantify mixing using an effective diffusivity based on a Lagrangian treatment of mixing and transformation of equations based on tracer-area coordinates. For this study, the former approach is followed on account of its directness. The isentropic eddy diffusivity is defined as the ratio of the net eddy transport of age to the mean meridional age gradient. The eddy age flux F_{eddy} is computed as the difference of total meridional age flux and the mean meridional advection of age by the mean flow. Mathematically, in isentropic coordinates, it is expressed as:

$$F_{eddy}(\phi,\theta) = \overline{\rho_\theta v \Gamma} - \overline{(\rho_\theta v)}\tilde{\Gamma} \tag{6}$$

where, $\tilde{\Gamma}(\phi,\theta) = \overline{\rho_\theta \Gamma}/\overline{\rho}_\theta$ is the mass weighted age in isentropic coordinates, ρ_θ is the isentropic density, v is the meridional velocity, and overbar denotes zonal averaging on fixed isentropes. The isentropic eddy diffusivity $\mathcal{D}_{eff}$ (units $\mathrm{m}^2\ \mathrm{s}^{-1}$) is then defined as the ratio of the density-scaled eddy flux and the meridional gradient of age as :

$$\mathcal{D}_{eff} = \frac{1}{\overline{\rho}_\theta}\frac{-F_{eddy}}{\partial_y \tilde{\Gamma}} \tag{7}$$

where $\partial_y = (1/R)\partial_\phi$ is the meridional gradient of the mean isentropic age. The eddy diffusivity is expected to peak in the stratospheric midlatitudes on account of strong planetary wave-induced eddy transport and weak meridional gradients in the surf zone. $\mathcal{D}_{eff}$ can therefore be used to qualitatively compare the structure of midlatitude eddy mixing.

3 Models

The revised mixing equation is tested using the two models introduced in Figure 1. The first is an idealized model with a prescribed equilibrium temperature profile, a simple treatment of gravity wave drag as a Rayleigh drag at the model top, and no other physical parameterizations in the stratosphere. The second is a comprehensive climate model with a detailed representation of chemistry and radiation. The models have similar numerics in that both employ a finite volume fluid dynamical solver, albeit on different horizontal grids. This eliminates a key source of uncertainty that can arise due to differences in model numerics itself (Gupta et al., 2020). Working with a comprehensive model and an idealized model also allows us to test how strongly the negative mix-

ing fluxes estimated using the vertical age gradient theory are related to complex parameterized processes.

3.1 Idealized Model: FV3

The study uses the Free Running model setup used in Gupta et al. (2020), with a finite volume dynamical core based on a cubed sphere grid. The core was developed at the Geophysical Fluid Dynamics Laboratory (GFDL) and is referred to as FV3 for short. The core employs finite volume schemes in both the vertical and the horizontal to solve the primitive equations (Putman & Lin, 2007). FV3 was built as the core of GFDL's Atmospheric Model, Version 3, AM3 (Donner et al., 2011), and a related non-hydrostatic version was recently adopted as the core of the National Center for Environmental Prediction Global Forecasting System. Further details on FV3 are provided in Gupta et al. (2020, Section 3 and Appendix A). Briefly, the model is driven with thermal forcings (Held & Suarez, 1994; Polvani & Kushner, 2002) detailed in Section 4.1 of Gupta et al. (2020). Newtonian relaxation to an analytically defined temperature state, which can be interpreted as a state of radiative-convective equilibrium, generates a perpetual northern-winter climatology. To quantify transport, a tracer with a concentration that is linearly increasing in time (a clock tracer) is introduced near the surface ($p \geq 700$ hPa) as detailed in Gupta et al. (2020), Section 4.1. The clock tracer is used to compute the age-of-air, which provides a measure of transport timescales of trace gases in the stratosphere.

As in Gupta et al. (2020), the model was integrated for 10,000 days and the last 3,300 days were used for transport analysis. The model was integrated at a $1^\circ \times 1^\circ$ horizontal resolution using a C90 horizontal grid with 80 σ-p hybrid levels in the vertical. The levels were pure-σ (terrain following) below 500 hPa, pure-pressure above 200 hPa and a linear combination of the two between 200 hPa ad 500 hPa.

3.2 Comprehensive Climate Model: WACCM

The comprehensive climate model employed in the study is the same as that employed in Linz et al. (2021): the Community Earth System Model 1 Whole Atmosphere Community Climate Model (WACCM), an interactive chemistry-climate model (Garcia et al., 2017; Marsh et al., 2013) developed at the National Center for Atmospheric Research (NCAR). This model uses physical parameterizations to represent complex earth

system processes including atmospheric chemistry and radiation, and is based on a finite-volume dynamical core (Lin, 2004) from the Community Atmosphere Model, version 4 (Neale et al., 2013). Its domain extends from the surface to 140 km, with 31 pressure levels from 193 to 0.3 hPa. The horizontal resolution is 2.5° longitude × 1.875° latitude, corresponding to the F19 horizontal grid.

The WACCM simulations are based on the Chemistry Climate Model Initiative REF-C1 scenario (Morgenstern et al., 2017). An ideal clock tracer, to compure the age-of-air, is included and is specified as in Garcia et al. (2011), with a uniform mixing ratio at the lower boundary that is linearly increasing in time. The model is forced with observed sea surface temperatures. The Quasi-Biennial Oscillation is nudged to observed winds, but otherwise the model evolves freely. The model was integrated from 1979 to 2014. Further details on WACCM are provided in Section 3 of Linz et al. (2021).

4 Results

The idealized FV3 model best allows us to contrast the original and revised mixing equation. Because it is in perpetual northern hemisphere winter, there is a continuous, strong mixing barrier associated with the Northern Hemisphere polar vortex. We therefore expect the assumptions of Linz et al. (2021) to be less appropriate than in a seasonally-varying context, where the annual breakdown of the vortex partially erodes the barrier. This experiment provides a more stringent test of our revised mixing formulation. Following that, we discuss our findings in the context of the comprehensive WACCM model.

4.1 Estimating the mixing fluxes using the refined theory

The climatological winds generated in response to the prescribed diabatic heating in FV3 comprises a strong polar vortex in the northern high latitudes and a strong easterly jet in the subtropics, Figure 3(a). The solid blue lines trace the turnaround latitude in each hemisphere, i.e. the latitude associated with zero diabatic velocity. The "tropical pipe" enclosed between the two blue curves is characterized by slow diabatic ascent of mass. Likewise, the region poleward of the blue curves is characterized by slow diabatic descent of mass. We refer to these two partitions as upwelling and downwelling regions respectively.

The climatological mean age-of-air profile (in color), obtained as a 10-year average, is well-stratified, monotonically increasing with height. At any given height, the youngest air is found within the tropics, and the oldest air either in the winter or summer polar region, depending on the level. The concave, vertically stacked contours in the equatorial region are consistent with slow vertical transport in the region; fresh air from the tropical tropopause is vertically advected upward. Away from the equator, the age increases monotonically and exhibits a strong gradient around the subtropical barrier. Poleward of the barrier, in the surf-zone, an abrupt flattening of the age contours is created by enhanced midlatitude mixing. In the winter hemisphere most of this mixing is induced by breaking planetary waves, while in the summer hemisphere it is induced by a combination of both synoptic-scale wave breaking in the lower stratosphere and slow diffusive transport elsewhere. In winter high latitudes, a steep increase in potential vorticity with latitude inhibits transport into and out of the polar vortex. Consequently, an abrupt increase in age is observed near the edge of the polar vortex.

The age-of-air in Figure 3(a) when weighted by the diabatic mass flux and averaged over the upwelling and downwelling regions, respectively, yields $\Gamma_u(\theta)$ and $\Gamma_d(\theta)$ (defined in equation 1), shown in Figure 3(b). The downwelling/midlatitude age, Γ_d, is older than the upwelling/tropical age, Γ_u, throughout the stratosphere, with the difference $\Delta\Gamma = \Gamma_d - \Gamma_u$ maximizing near 500 K in the lower stratosphere.

The mixing equation, Equation 2, connects the net vertical aging of air in the tropical pipe to the aging by diabatic advection vs adiabatic mixing. The net aging, i.e., the vertical gradient of the upwelling age (T1), is maximum near 400 K, above which it monotonically decreases with height, Figure 3(c). In the lower stratosphere, a major fraction of the aging can be attributed to mixing in the lower stratosphere, as shown in Figure 3(d) (solid curve). The other factor contributing to the aging is the reduction of vertical motion on account of increased static stability as compared to the troposphere. At 400 K, the bulk mixing term (T3) accounts for an aging rate of 0.018 yr K^{-1} out of the net vertical aging (T1) of 0.028 yr K^{-1}, Figure 3(c), as the synoptic-scale mixing dominates in both the hemispheres. This fraction, however, rapidly decreases with height and between 550-600 K almost all the aging is accounted for by the advective term (T2). In fact, our computations yield slightly negative values of the bulk mixing term in this region, a clearly nonsensical result. In the upper stratosphere, the increase in the relative

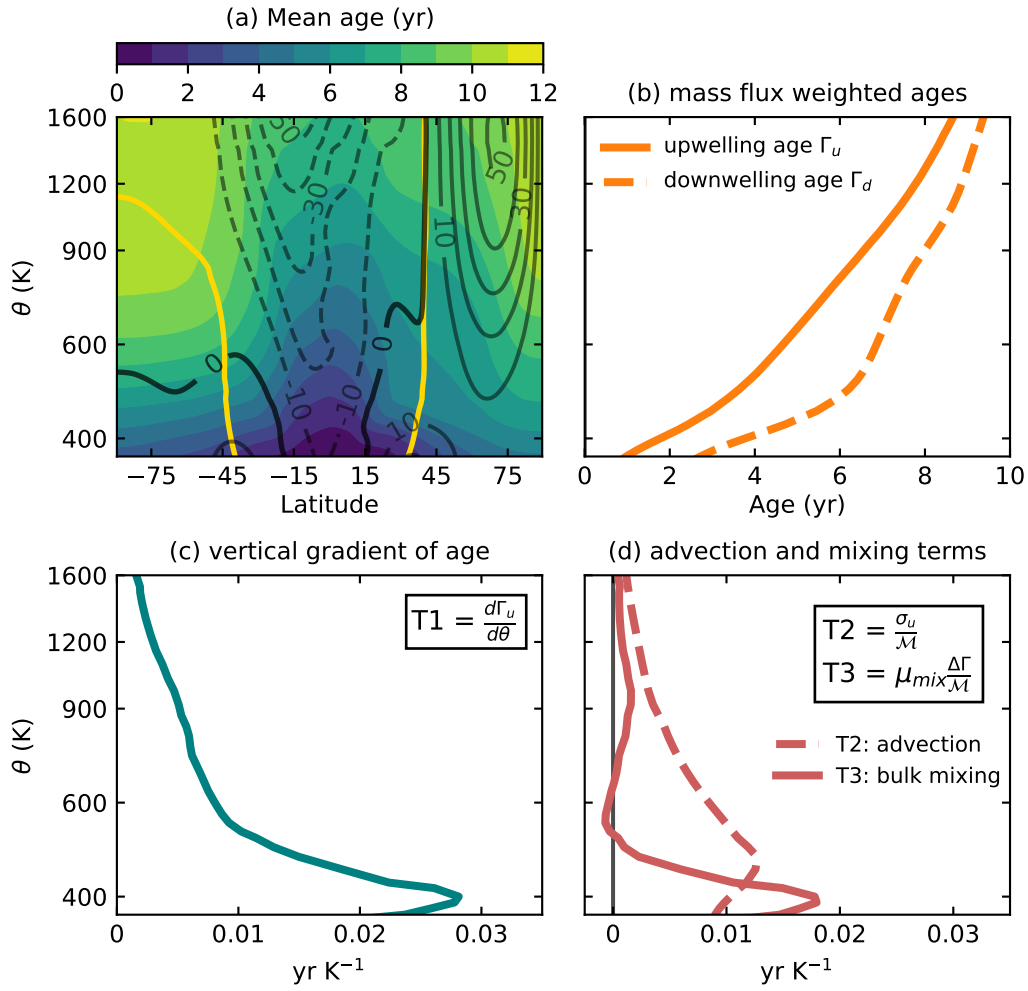

Figure 3. (a) The climatological mean age profile (in color) and zonal mean zonal wind (in black), along with the zero diabatic velocity curve (in yellow) for the FV3 idealized model. (b-d) Individual terms of Equation 2 applied to the idealized model: (b) The diabatic flux weighted upwelling and downwelling ages, Γ_u (solid) and Γ_d (dashed), (c) the vertical gradient of upwelling age, $\partial\Gamma_u/\partial\theta$, i.e., term T1 in the mixing equation, and (d) advection (dashed) and bulk mixing (solid) terms i.e., terms T2 and T3 in the equation respectively. The term T3 is computed as the difference T1-T2, leading to spurious, negative values for the bulk mixing flux μ_{mix}.

contribution by the bulk mixing term is due to enhanced mixing due to breaking planetary waves.

As was pointed out in Linz et al. (2021) and also shown in Figure 1, minor negative fluxes are obtained in the middle stratosphere both for the comprehensive WACCM

model (annual average) and for the idealized FV3 model. This "negative mixing" is not a numerical artifact but rather a consequence of the assumption of fast horizontal mixing within both the upwelling and downwelling regions. While this assumption allows convenient assessment of age in the two regions using characteristic values Γ_u and Γ_d, it ignores the meridional gradient in age around the subtropical transport barrier. The flux of older midlatitude air into the tropics is localized around the barrier itself, barely churning the air in the deep tropics.

The bulk mixing term (T3) and bulk mixing flux μ_{mix} in Equation 2 are computed as residual terms in the mixing equation. To first verify that the mixing is always positive, we compute the meridional profile of the eddy flux of age, F_{eddy}, was computed and is shown in Figure 4(a) (in color). F_{eddy} is computed from the eddy covariance in isentropic coordinates, as in Equation 6. Negative and positive fluxes in the winter and summer hemisphere respectively indicate an equatorward transport of age by midlatitude eddies. In the winter hemisphere, the eddy age flux has a two-peaked structure in the vertical, with the first maximum at 425 K in the lower stratosphere (due to synoptic-scale mixing) and the second maximum at around 1000 K in the upper stratosphere (due to planetary-scale mixing). This structure mirrors the two-peaked mixing efficiency structure obtained by Gupta et al. (2021) and shown in Figure 1(b). Substantially weaker eddy flux is found in the 550-650 K region — the region where negative μ_{mix} is obtained using Equation 2 — but the flux is always equatorward. Weak mixing in this region is consistent with past studies (e.g. Shuckburgh et al. (2001)) which employ other metrics to quantify stratospheric mixing over a shorter time period.

The dashed black contours in Figure 4(a) show the corresponding eddy diffusivity, $\mathcal{D}_{eff}$ (defined in Equation 7). Focusing on the winter hemisphere, large values of the eddy diffusivity around the turnaround latitude (solid black) indicates that most of the mixing is indeed localized around the turnaround latitude. This validates the use of the turnaround latitude to compute the midlatitude mixing flux. The diffusivity is substantially lower within the tropical pipe indicating minimal mixing of midlatitude air into the deep tropics (15°S to 15°N).

The wintertime eddy diffusivity is overlaid on to the age-of-air profile on the 550 K isentrope using a thick orange highlighting in Figure 4(b), an isentrope height associated with negative mixing (Figure 1). The bold orange curve highlights the latitudes

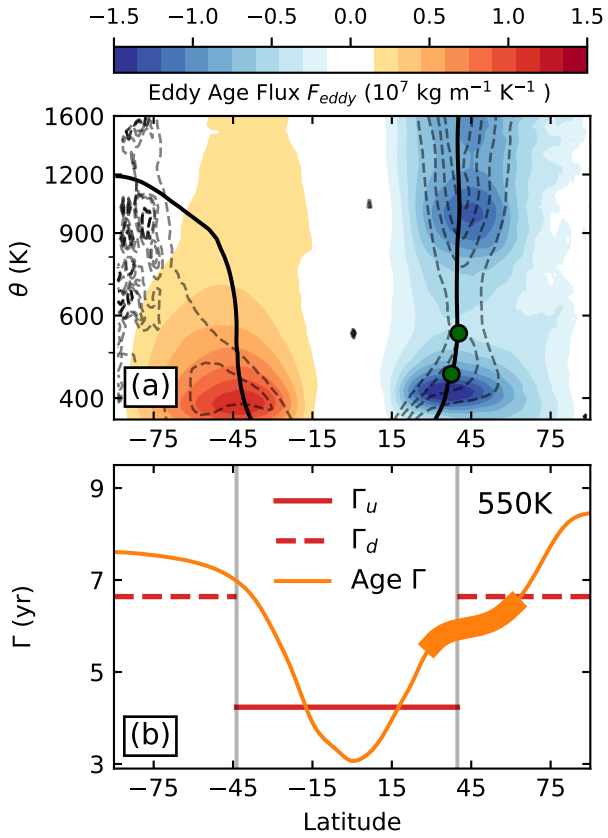

Figure 4. (a) Eddy flux of age, F_{eddy} (in color), and eddy diffusivity $\mathcal{D}_{eff}$ (in dashed), for idealized model stratosphere. The solid black curve traces the region with net zero diabatic velocity. The eddy diffusivity has units of m^2 s^{-1} and is shown at contour intervals of 0.75 × 10^6 m^2 s^{-1}. (b) Zonal mean age profile on the 550 K isentropic level for the idealized model (thin orange). The solid and dashed red line in the tropics and extratropics show the weighted ages Γ_u and Γ_d respectively, and the bold orange curve in the northern extratropics highlights the region with strong eddy diffusivity, i.e., 10% and higher of the maximum diffusivity at 550 K. The vertical grey bars show the turnaround latitude, demarcating the regions of upwelling and downwelling.

associated with strong eddy diffusivity, defined as values 10% or higher than the maximum diffusivity on a given level. Most of the mixing occurs between 30°N and 60°N, exchanging parcels with age over a range of 5.5 years to 6.8 years. This range is overestimated by the mixing theory which instead assumes that the tropical parcels with age $\Gamma_u = 4$ Yr (solid red bar) mix with the extratropical parcels with age $\Gamma_d = 6.8$ Yr (dashed red bars). These ages correspond to the latitudes 15°N and 60°N respectively. The age

difference $\Delta\Gamma$ between the parcels being mixed between the upwelling and downwelling regions is overestimated in the assumptions leading to Equation 2, which causes the mixing flux, μ_{mix}, to be underestimated.

We next demonstrate that a better estimation of the age difference mixed across the mixing barrier is indeed crucial for quantifying the mixing flux; especially in the middle and lower stratosphere. We quantify the actual age range of parcels being mixed near the partition boundary with the Γ-θ circulation, ψ (defined in Equation 4) was computed for the dry dynamical core FV3 using daily samples over a 3300-day period. The circulation ψ at 450 K for FV3 is shown in Figure 5(a). Latitude and ages with a non-zero circulation strength (in color) show the latitudes that exhibit tracer transport by midlatitude eddies and the age of parcels being transported at those latitudes. In the northern hemisphere, a positive ψ signifies a poleward mass transport. Figure 5(a) shows the predominantly bidirectional transport of mass in the midlatitudes in FV3. For age values less than the mean isentropic age (solid black), a positive (teal colored) circulation cell means that the eddies transport younger age poleward. Likewise, for ages older than the mean age, a negative (brown colored) circulation cell means that the eddies transport older age equatorward.

The range of age values being mixed is the highest in the winter midlatitudes, consistent with the predominant wave-mixing over a large spatial scale. Moreover, the circulation peaks in the vicinity of the turnaround latitude. The circulation in the vortex region is considerably weaker, on account of the vortex being isolated from the midlatitudes. The age range of the streamfunction is markedly narrower in the subtropical latitudes, which are characterized by weak adiabatic mixing, virtually going to zero at the equator. The distribution in the summer midlatitudes (not shown) is qualitatively similar to the winter midlatitudes, except that mixing at higher altitudes occurs over a narrower age range, i.e., over a narrower range of latitudes.

Focusing around the turnaround latitude in the winter hemisphere (dashed black vertical bars; $\approx$37.4° N) — where the mean isentropic age is 5.2 Yr (solid black) — the poleward transport of mass (teal) carries parcels with ages between 3 to 5.2 Yr from the subtropics to higher latitudes. Likewise, the equatorward flux (brown) carries parcels with ages between 5.2 Yr to 6.5 Yr from higher latitudes into the subtropics. Nearly all of the circulation near the turnaround latitude is associated with carrying parcels with age in

the 4-6 Yr range, implying that a majority of parcels being carried poleward have age between 4 and 5.2 Yr, and the majority of parcels being carried equatorward have age between 5.2 to 6 Yr. This is seen more clearly in Figure 5(b) which shows a cross-section of ψ along the dashed black bar in Figure 5(a) at the turnaround latitude of 37.4°N (blue curve); by fixing both θ and ϕ, ψ is now a function of age alone. The asymmetric circulation distribution strongly tapers off away from the mean isentropic age of 5.2 Yr in either direction. It confirms that most of the mixing at this latitude occurs among parcels with age not younger than 4 Yr but also not older than 6 Yr.

The average age transported from the subtropics to the midlatitudes (and vice versa) can be computed by calculating the ψ-weighted mean age exclusively over the region of positive (negative) Γ-θ circulation. Using the terminology introduced in Section 2, this weighted age-of-air actually being mixed at 450 K represented as $\Gamma_{u,eff}$ (and $\Gamma_{d,eff}$) is shown using the solid (dashed) green vertical bars in Figure 5(b). Here, $\Gamma_{u,eff}$= 4.2 Yr and $\Gamma_{d,eff}$= 5.6 Yr. Thus, the effective age difference mixed across the barrier is $\Delta\Gamma_{eff} = \Gamma_{d,eff} - \Gamma_{u,eff}$ = 1.4 Yr. This age difference is approximately half of the age difference $\Delta\Gamma$ = 2.5 Yr between the ages Γ_u = 3 yr (solid red) and Γ_d = 5.5 yr (dashed red) assumed while deriving Equation 2. This correction implies that the bulk mixing flux μ_{mix} underestimates the actual exchange flux by about 50%. Accordingly, the perturbation age $\delta\Gamma_u = \Gamma_{u,eff} - \Gamma_u$ = 1.2 Yr, and $\delta\Gamma_d = \Gamma_d - \Gamma_{d,eff}$ = -0.1 Yr are obtained.

We can use the effective mixing ages to quantify the range of mixing. Referring to the mean age in subplot (a), the inferred values for $\Gamma_{u,eff}$ and $\Gamma_{d,eff}$ suggest that the mixing predominantly occurs between 25°N and 55°N, instead of 15°N and 55°N as the red bars would indicate. Mixing is localized near the mixing barrier and the deep tropics are fairly isolated from the mixing flux originating in the midlatitudes.

Figure 5(c) shows the Γ-θ circulation at the 550 K isentropic height. At this level, $\Gamma_{u,eff}$= 5.1 Yr and $\Gamma_{d,eff}$= 6.3 Yr, and thus $\Delta\Gamma_{eff}$ = 1.2 Yr. With Γ_u= 4.2 Yr and Γ_d= 6.6 Yr, $\Delta\Gamma$ = 2.4 Yr. Similar to 450 K, at 500 K the corrected age difference $\Delta\Gamma_{eff}$ is approximately half of $\Delta\Gamma$, and perturbation age $\delta\Gamma_u$ = 0.9 Yr and $\delta\Gamma_d$ = 0.3 Yr are obtained.

The procedure was repeated for all the isentropic levels, i.e., the Γ-θ circulation was used to compute the distribution of ages being mixed at the turnaround latitude in the winter hemisphere. The distribution was used to estimate $\Gamma_{u,eff}$ and $\Gamma_{d,eff}$, which were

ultimately used to obtain the perturbation ages $\delta\Gamma_u$ and $\delta\Gamma_d$ at each vertical level. This allows us to calculate all the variables except μ^T_{mix} in the refined mixing equation (Equation 3), and ultimately compute μ^T_{mix} as a residual.

The structure of the "effective" upwelling and downwelling age-of-air being exchanged is shown in Figure 6(a) (black curves). The analysis using the Γ-θ circulation reveals that influence of meridional gradients to the mixing estimation is the strongest in the lower stratosphere in the tropics and in the middle stratosphere in the extratropics. The weighted age Γ_u (solid orange) and the effective mixing age $\Gamma_{u,eff}$ (solid black) in Figure 6(a) differ the most between 400 K and 600 K, and thus $\delta\Gamma_u$ peaks in this interval. The corresponding midlatitude ages (dashed curves), however, differ the most between 500 K to 900 K, and so $\delta\Gamma_d$ peaks in this interval.

Our analysis also shows prominent differences between the original age difference $\Delta\Gamma$ and the effective mixing age difference $\Delta\Gamma_{eff}$ (Figure 6(b)). Throughout the lower and middle stratosphere, a significant reduction in the age difference is observed, indicating that the difference in the mean poleward and the mean equatorward moving age is indeed much lower than the assumed mixing age difference $\Delta\Gamma$. It should be noted that the two measures are found to be almost indistinguishable in the upper stratosphere, but elsewhere, the true age difference being mixed is overestimated by at least 50%. Note that this has no implications for the diabatic circulation strength, which is still directly related to $\Delta\Gamma$ (Linz et al., 2016).

Finally, we consider the new "entrainment freshening" term (C4) in the refined mixing equation and assess its contribution to the net aging in the tropics. The quantity, shown in Figure 6(d), is consistent with a peak in $\delta\Gamma_u$, and contributes most to the aging in the lower stratosphere. Note the negative sign in front of C4 in Equation 3, meaning that a positive C4 leads to a reduction in aging. The key is that the air being expelled from the tropics is older than the mass flux weighted age Γ_u: entrainment "freshens" the pipe by ejection of older air. The term is positive even around 600 K, where very weak (and even negative mixing) was estimated for the FV3 core (Figure 1). The positive value of the term C4 in this region can explain the spurious "negative" mixing observed in the bulk flux. With a lower stratospheric peak of 0.013 yr/K, this entrainment freshening term significantly reduces the overall aging. Comparing this term with the net vertical aging in Figure 3(c) and the advection term in Figure 3(d) reveals that

the entrainment freshening term C4 contributes a substantial fraction to the net aging in the tropics. In fact, in the 400-500 K range, the magnitude of this term is more than half as large as the net aging (comparing the green curve in Figure 6(d) and the teal curve in Figure 3(c)), reaffirming our hypothesis.

We now compare the "bulk" mixing fluxes obtained from Equation 2 with the "true" mixing fluxes obtained from Equation 3. To do this, the mixing efficiency ϵ, which measures the strength of the mixing flux relative to the net poleward flux, is used: $\epsilon = \mu_{mix}/\mu_{net}$. Using the refined mixing equation to estimate the mixing fluxes leads to a striking enhancement in the mixing efficiency in FV3 (Figure 7(c)). A positive age perturbation $\delta\Gamma_u$ in the region leads to a positive offset in the mixing flux. Moreover, a markedly lower age difference $\Delta\Gamma_{eff} < \Delta\Gamma$ results in a multiplied (magnified) mixing flux μ^T_{mix}. The entrainment freshening term (C4) ensures a non-negative mixing flux throughout the stratosphere, while the adjustment to $\Delta\Gamma_{eff}$ increases the amplitude of the flux. The original mixing equation yielded an erroneously weaker ϵ (thin dashed red) in the lower stratosphere than the ϵ computed from the refined mixing equation (thick solid red). As will be discussed in more detail later, the revised mixing efficiency (and thus the mixing flux) bears a much stronger resemblance to the mixing efficiency obtained from the comprehensive model WACCM.

4.2 Estimating the meridional extent of adiabatic mixing

We now address the question that naturally follows: What then is the region over which the air is truly mixed in the winter stratosphere? The estimates $\Gamma_{u,eff}$ and $\Gamma_{d,eff}$ of the true ages of the parcels mixed across the turnaround latitude can be mapped to the latitudes with the corresponding mean age Γ. That is, we find the latitudes $\phi_1(\theta)$ and $\phi_2(\theta)$ such that the zonal mean age $\Gamma(\phi_1(\theta), \theta) = \Gamma_{u,eff}(\theta)$ and $\Gamma(\phi_2(\theta), \theta) = \Gamma_{d,eff}(\theta)$. The two latitudes obtained by the mapping provide the equatorward and poleward extent of the midlatitude mixing. The results for FV3 from this procedure are shown in Figure 8(a) (orange curves and shading). Throughout much of the stratosphere, the region of mixing (orange shading) roughly spans from 20°N to 60°N. The most notable feature obtained is that the mixing region is shifted poleward in the 400-500 K interval. In addition, above 600 K, a steady but small widening of the mixing region is noted.

Comparing this with the region deduced from gross upwelling ages Γ_u and Γ_d (dashed black curves and shading), we find that the most prominent differences appear in the 400-700 K region, where the blue curve in the subtropics aligns more strongly with the sharp subtropical age gradient while the dashed black curve does not. This is readily observed in the 450-500 K height range. Between 400-700 K, the Linz et al. (2021) theory assumes the mixing to dominate over a wider region in the subtropics. However, the opposite is suggested above 700 K. Here, Linz et al. (2021) theory assumes mixing to be restricted to poleward of 25° N, presenting a contrast to a boundary of 20° N proposed by the refined theory.

The poleward boundary of mixing, however, is not as sensitive to the definition used. In the lower stratosphere, the solid blue and dashed black curves from the two definitions tend to be nearly identical. Some small but notable differences emerge only above 500 K where the corrected ages suggest that the mixing is restricted to relatively lower latitudes than that expected by the original Linz et al. (2021) theory. Even though both estimates suggest that the mixing regions are not significantly different, it is surprising how much impact even such small differences can make to the mixing flux estimates in the lower stratosphere; purely on account of strong sub-tropical gradients in the age-of-air profile.

4.3 Insights from the WACCM Comprehensive Climate Model

The analysis was repeated for WACCM, which provides a more Earth-like representation of stratospheric variability and seasonal cycle. The northern winter months of November to March were considered for a period of five years and daily samples were used to compute the age-of-air and the Γ-θ circulation. The more limited data, coupled with more internal variability, leads to more sampling uncertainty in these calculations.

We first emphasize that the zonal mean age-of-air in WACCM (shown later in Figure 8(b)) is much younger than in FV3 both on account of a faster circulation and a higher tropopause, and because the age in WACCM is computed w.r.t. the tropical stratosphere, i.e., the whole troposphere is the source. In FV3 the age-of-air is computed w.r.t the source region of 700 hPa and below, due to which the age at the tropical stratosphere has a mean value of approx. 1 year. This offset does not affect the results in this study, as the differences in age are dominated by the differences in circulation.

The Γ-θ circulation in WACCM at the 450 K isentropic height is shown in Figure 5(d). Comparing subplots (a) and (d), the gross structure of ψ is quite similar between the idealized dry dynamical core and WACCM. The circulation peaks in the midlatitudes and is weaker elsewhere. Moreover, for latitudes with considerable circulation strength, parcels with age younger than the mean age (solid black) are carried poleward and parcels with age older than the mean age are carried equatorward. Little to no circulation is noted in the polar regions on this isentropic surface.

The cross section of ψ at 450 K along the turnaround latitude of 32.6°N in the winter hemisphere (dashed black bar in Figure 5(d)) is shown in Figure 5(e). Yet again, we find that the gross structure of ψ is very similar between WACCM and FV3 (Figure 5(b)). The Γ-θ circulation is informative of the broad range of ages of parcels being mixed around the barrier. At 450 K, parcels as young as 0.5 Yr are mixed with parcels with age up to 2.5 Yr. A considerable portion of the mixing, however, occurs between parcels with age $\Gamma_{u,eff}$= 0.9 Yr and $\Gamma_{d,eff}$= 2 Yr (solid and dashed green respectively). Computations yield $\delta\Gamma_u$=-0.05 Yr and $\delta\Gamma_d$=0.75 Yr.

The most conspicuous difference between the mixing in FV3 and WACCM on 450 K is that in FV3, Γ_u and $\Gamma_{u,eff}$ are quite different, while Γ_d and $\Gamma_{d,eff}$ are almost identical (Figure 5(b)). In contrast, for WACCM, it is the Γ_u and $\Gamma_{u,eff}$ which are almost identical and the downwelling ages Γ_d and $\Gamma_{d,eff}$ which are quite different. So, the (relatively weaker) subtropical gradients barely impact the estimation of the tropical age being mixed. Nevertheless, the Γ-θ circulation in both the models suggest that the true age difference mixed around the turnaround latitude is much lower than the bulk age difference $\Delta\Gamma$, with most of the difference coming from the downwelling ages.

Next, the Γ-θ circulation at 550K is shown in Figure 5(f). At this level, parcels with stratospheric age as young as 2 Yr are mixed with parcels with age as old as 4 Yr. However, the bulk of the mixing occurs between ages $\Gamma_{u,eff} = 2.4$ Yr and $\Gamma_{d,eff} = 3.4$ Yr, yielding an effective mixed age difference $\Delta\Gamma_{eff} = 1$ Yr, much less than a $\Delta\Gamma = 1.4$ Yr. It follows that $\delta\Gamma_u \approx 0$ and $\delta\Gamma_d = 0.4$ Yr. Similar to 450 K, a weak perturbation age $\delta\Gamma_u$ on 550 K is obtained for WACCM.

Similar to FV3, the wintertime averages of all the terms in the refined mixing equation were computed for WACCM. Here, we only show the effective age difference $\Delta\Gamma_{eff}$ (Figure 6(c)) and the entrainment freshening term C4 for WACCM (violet curve in Fig-

ure 6(d)); terms which are associated with the revised mixing equation. Our estimate for $\Delta\Gamma_{eff}$ using the Γ-θ circulation shows a considerably smaller age difference being mixed across the turnaround latitude; Therefore, for both FV3 and WACCM, $\Delta\Gamma_{eff} << \Delta\Gamma$.

The entrainment freshening term for WACCM (violet curve in 6(d)) is weaker and unlike FV3, barely contributes to the net vertical aging in the lower stratosphere. This is due to the fact $\Gamma_u \approx \Gamma_{u,eff}$ in WACCM; the air being entrained into the extratropics carries the mean age with it. In fact, the quantity is nearly vanishing throughout the stratosphere, indicating that entrainment freshening does not have a strong effect on the mixing flux estimation in WACCM. Since C4 is weakly negative in the lower stratosphere, a smaller mixing term (C3) leads to a slight reduction in the "true" mixing flux estimated from Equation 3. We believe, however, that the entrainment mixing term is not sufficiently sampled due to limited data availability for WACCM. The $\Gamma - \theta$ circulation is sensitive to the sampling frequency and sample size, more so than the other dynamical quantities in the revised mixing equation. Sampling the streamfunction at a frequency higher than the timescales associated with isentropic mixing is crucial to obtaining a smooth streamfunction profile. Since the entrainment freshening term is weak and not always physically consistent, we neglect this term and only consider the effective age difference while computing the revised mixing efficiency for WACCM.

The figure shows the bulk and true mixing efficiency computed for WACCM. Both the bulk and true mixing efficiency in WACCM (in dashed and bold gray respectively) have similar gross structure throughout the stratosphere. The two mixing profiles differ in that the true mixing is more enhanced in the lower stratosphere. $\Delta\Gamma_{eff}$ which is smaller than $\Delta\Gamma$ results in enhancement of the mixing fluxes in lower and middle stratosphere. A stronger mixing in WACCM is also consistent with a stronger wintertime circulation in WACCM. The bold grey curve suggests a mixing efficiency of 2 in the lower stratosphere. This is equivalent to the true mixing flux μ_{mix} being two-thirds the strength of the equatorward mass flux.

The same procedure as described in Section 4.2 was applied to WACCM in order to estimate the latitudinal span of wave-induced mixing. Figure 8(b) shows the mixing span estimated for WACCM using both $\Gamma_{u,eff}, \Gamma_{d,eff}$ (orange curves and shading) and Γ_u, Γ_d (dashed black curves and shading). The two types of ages yield regions which are different in structure. The region determined from corrected ages spans from 20°N to

45°N in the lowermost stratosphere (400K) and gradually decreases in width up to 700 K where it only spans from 15°N to 35°N. Most notable is the equatorward shift in the orange curve in the subtropics, in phase with the turnaround latitude (solid black). Above 700 K, the region re-widens, spanning all the way from the equator on the left to 60°N on the right. We note that above 1100 K the corrected tropical age $\Gamma_{u,eff}$ is younger than the equatorial age and thus the mixing span has been truncated at the equator. Such young ages are most likely obtained due to (i) rapid equatorward shift of the turnaround latitude with height, (ii) transience in the zonal mean age at lower latitudes in WACCM, and (iii) prevailing inter-hemispheric transport.

In contrast, the mixing span determined from Γ_u, Γ_d spans from 20°N on the equatorward side to 70°N on the poleward side. This range is considerably wider than that for FV3 (black shading in subplot (a)). Interestingly, for FV3, both the dashed black curves lay on either side of the turnaround latitude. This is not the case for WACCM, where the turnaround latitude makes a drastic equatorward turn. Since the corrected ages were inferred by analyzing the Γ-θ circulation around the turnaround latitude, differences in the diabatic velocity structure between FV3 and WACCM lead to major differences obtained between the orange and black shaded regions as well in WACCM. Despite these differences, it is found that the deep tropics barely witness any wave-induced adiabatic mixing and are fairly isolated, just as in FV3.

In summary, the structure of the Γ-θ circulation is similar for FV3 and WACCM, and both models demonstrate an overestimation of the mixed age difference in the original mixing equation. Employing the refined mixing theory, which estimates the age difference more accurately, yields similar mixing efficiency ϵ for the two models. Limited sampling in WACCM may also contribute slightly to the observed differences between FV3 and WACCM. Only 5 years of daily data, 150 days per year, was considered from WACCM. This is significantly lower than 10 years of data, 360 days per year, considered for the dynamical core. Moreover, the original mixing equation of Linz et al. (2021) assumes a stratosphere in steady state, and for WACCM the NDJFM climatology is coupled with the effects of dynamics and transport during other seasons. The choice of perpetual solstice climatology in FV3 ensures that contributions from inter-seasonal variability are eliminated in the analysis and the circulation is statistically steady. Some differences in mixing may also be due to the presence of a nudged QBO in WACCM vs persistent tropical easterlies in FV3.

5 Discussion and Conclusions

Wave-induced adiabatic mixing plays a key role in mixing trace gases over large spatial scales in the winter stratosphere, and in influencing their global distribution. Accurately quantifying this mixing is key to understanding transport trends in the stratosphere in a changing climate. We have proposed a method to improve the estimates of the adiabatic mixing flux in the stratosphere obtained from applying the vertical age gradient theory of Linz et al. (2021), and have used it to quantify the extent of mixing between the tropics and midlatitudes. We show that the deep tropics do not participate in the adiabatic mixing of tracers in most of the stratosphere.

The theoretical formulation of Linz et al. (2021) partitions the stratosphere into regions of diabatic upwelling and diabatic downwelling. This allowed them to connect the vertical gradient of tracer (age-of-air) in the upwelling region (tropics) with the quasi-horizontal adiabatic mixing flux between the two partitions, thus allowing computation of the mixing flux using tracer-based measures. The theory assumes fast mixing within both the tropics and the extratropics, and hence neglects any gradients in age-of-air profile expected near the subtropical transport barrier. We show that this assumption leads to an overestimation of the meridional span of adiabatic mixing in the winter stratosphere, and as a result, an underestimation of the mixing fluxes. We refined the framework in order to include the effects of meridional age gradients. This allows a more comprehensive estimation of the age of the air parcels exchanged between the upwelling and downwelling partitions of the stratosphere. We used the refined age mixing theory to quantify the meridional span of adiabatic mixing in the winter stratosphere.

The correction was made possible by a novel strategy to obtain the complete age range of air parcels mixed around the turnaround latitude through the Γ-θ circulation streamfunction. The streamfunction is essentially a joint distribution which allows quantification of mass transport in the latitude-age-isentrope space; i.e, at a given latitude and isentropic height, what fraction of the total mass transport is associated with a given age? Having information of the age-of-air distribution being mixed enabled estimation of the "true" ages that are mixed around the winter hemisphere turnaround latitude. We calculated the true difference in the age-of-air being transported from upwelling to the downwelling region and vice versa, and found that this effective age difference is significantly smaller than the age difference assumed in the Linz et al. (2021) theory.

The true ages of air being mixed was used to re-derive the mixing equation of Linz et al. (2021) (Equation 2) to yield Equation 3, which accounts for age gradients as well. The new mixing equation replaces the gross age differences $\Delta\Gamma$ of the mixed parcels with the revised age difference calculated from the Γ-θ circulation. It also contains an additional advection term (the entrainment freshening) that captures the effects of entrainment on the tropical age in the presence of subtropical gradients.

For a thorough test of the proposed theory, we considered both an idealized model, a dry dynamical core and a comprehensive model. Both of these choices were made to maximize the error that will be introduced into the original mixing theory, as averaging over several years of seasonally-varying circulation (as in Linz et al. (2021)) will damp the effects highlighted here. Both the models exhibit similar Γ-θ circulation, qualitatively, in the lower stratosphere. Further, results from both models indeed verify an overestimation of the age difference $\Delta\Gamma$ mixed between the upwelling and downwelling regions by the original mixing equation. On applying the revised mixing theory to the models, it was found that both the idealized and the comprehensive model qualitatively produced very similar mixing efficiencies (a proxy for mixing fluxes).

The models show a strong agreement throughout the stratosphere. In fact, we highlight that both models also agree that the deep tropics, from the equator all the way to 15°N, is fairly isolated from adiabatic mixing and that the equatorial region almost exclusively experiences pure diabatic advection of air. This is especially true in the lower and the middle stratosphere. Our findings corroborate the findings from an independent study by the co-authors Curbelo and Linz, who used Langrangian trajectories to quantify the mixing of midlatitude air into the tropics.

We conclude that our analysis highlights both the sensitivity of the mixing flux to the strong age gradients near the turnaround latitude, and their importance in the estimation of the quasi-horizontal mixing flux. It also demonstrates that tracer-based measures can be used to estimate the meridional span of adiabatic mixing in the winter midlatitudes given sufficiently detailed data. The theory proposed in this study can be used to quantify mixing in the observed stratosphere as well, using both satellite observations and reanalyses, especially in the lower and middle stratosphere. Past studies have used transport models and specified dynamics to compute and compare the mean age-of-air across different reanalyses (Chabrillat et al., 2018; Ploeger et al., 2019). Our analysis could

be further used to connect the impact of differences in adiabatic mixing to the observed age differences, and over a longer timescale than those considered in this study, using more than forty years of reanalyses.

Projecting the mass transport into latitude-age-isentrope space using the Γ-θ circulation presents a new way to assess the adiabatic mixing structure in the stratosphere. The streamfunction couples the dynamics and transport into a single quantity, and instead of age-of-air tracer, it could be generalized to any chemical trace gas species with weak sources and sinks in the stratosphere: nitrous oxide, sulphur hexafluoride and methane, for example. The circulation distribution can be of value in investigating transport exchanges across the wintertime polar vortex, or mixing in the upper troposphere lower stratosphere (UTLS) region where the combined effects of stratosphere-troposphere mass exchange, convection and jet instability, influence the ozone and water vapor reservoirs.

Appendix A Revised Mixing Equation

The age-of-air is an idealized tracer with no spatial sources and sinks away from the boundary. The age tracer only has a source in time, i.e., the age of a parcel in the free atmosphere ages at a rate of 1 second per second. Therefore, for a stratosphere in steady state, the tracer continuity equation for the age-of-air, following Linz et al. (2016), can be generally written as :

$$\frac{1}{\rho_\theta}\nabla \cdot \mathcal{F} = 1 \tag{A1}$$

where $\rho_\theta = \frac{-1}{g}|dp/d\theta|$ is the three-dimensional isentropic density, and $\mathcal{F}$ is the net advective-diffusive mass flux of age. Considering a stratospheric air mass enclosed between two isentropes θ and over $\theta+\Delta\theta$ in the vertical and spanning the whole upwelling partition in the horizontal, the net age budget for the box (or layer) can be, most simply, written as :

$$\text{Age Flux Out} = \text{Age Flux In} + \text{Source} \tag{A2}$$

Mathematically, this is equivalent to multiplying Equation A1 by ρ_θ, and horizontally integrating both sides over the upwelling region and over the isentropes θ and $\theta+\Delta\theta$ in the vertical. Assuming the contribution from diffusion to be small, all the fluxes

take an advective form. Adopting the terminology introduced in Linz et al. (2021) and in Section 2, the total age flux entering the box is the sum of the upward directed diabatic flux of age entering the box from below (i.e. the θ isentrope) and the adiabatic advective flux of older age $\Gamma_d - \delta\Gamma_d$ by the mixing flux μ_{mix} from the downwelling region. Similarly, the total age flux exiting the box is the sum of the upward directed diabatic flux of age exiting the box from the top (i.e. the $\theta+\Delta\theta$ isentrope) and the poleward advective flux of $\Gamma_u + \delta\Gamma_u$ by the entrainment μ_{ent} into the downwelling region. Both μ_{mix} and μ_{ent} have units of kg/s/K (mass flux per unit isentropic height). The tracer continuity equation for the infinitesimal layer can thus be written as :

$$\Gamma_u \mathcal{M}_u(\theta+\Delta\theta) + \int_{\theta}^{\theta+\Delta\theta} \mu_{ent}(\Gamma_u + \delta\Gamma_u)\, d\theta = \int_{\theta}^{\theta+\Delta\theta} \mu_{mix}(\Gamma_d - \delta\Gamma_d)\, d\theta + \Gamma_u \mathcal{M}_u(\theta) + \int_{\theta}^{\theta+\Delta\theta} \rho_\theta d\theta \tag{A3}$$

We rearrange and express $\Gamma_u \mathcal{M}_u(\theta + \Delta\theta) - \Gamma_u \mathcal{M}_u(\theta)$ as $\Delta\theta \cdot d(\Gamma_u \mathcal{M}_u)/d\theta$ and apply the product rule to get the left hand side of Equation A4. In addition, we approximate the integrals by multiplying the integrand by $\Delta\theta$. Cancelling $\Delta\theta$ from each side, we get :

$$\Gamma_u \frac{d\mathcal{M}_u}{d\theta} + \mathcal{M}_u \frac{d\Gamma_u}{d\theta} = -\mu_{ent}(\Gamma_u + \delta\Gamma_u) + \mu_{mix}(\Gamma_d - \delta\Gamma_d) + \sigma_u \tag{A4}$$

where σ_u is the isentropic density horizontally integrated over the upwelling region (units kg/K). By mass continuity, $\mu_{net} = -\frac{d\mathcal{M}_u}{d\theta}$, and by definition, $\mu_{net} = \mu_{ent} - \mu_{mix}$. On substitution and rearranging, we get :

$$\frac{d\Gamma_u}{d\theta} = \frac{\sigma_u}{\mathcal{M}_u} + \frac{\mu_{mix}(\Delta\Gamma_d - \delta\Gamma_d - \delta\Gamma_u)}{\mathcal{M}_u} - \frac{\mu_{net}\delta\Gamma_u}{\mathcal{M}_u} \tag{A5}$$

For a steady state circulation, the upwelling mixing flux balances the downwelling mixing flux and thus, $\mathcal{M}_u = -\mathcal{M}_d = \mathcal{M}$. On substitution, this yields the revised mixing equation A6, identical to Equation 3 :

$$\frac{d\Gamma_u}{d\theta} = \frac{\sigma_u}{\mathcal{M}} + \mu_{mix}\frac{\Delta\Gamma_{eff}}{\mathcal{M}} - \mu_{net}\frac{\delta\Gamma_u}{\mathcal{M}} \tag{A6}$$

Acknowledgments

We thank Hella Garny and Thomas Birner for insightful suggestions. WACCM is a component of the Community Earth System Model (CESM), which is supported by the National Science Foundation (NSF) and the Office of Science of the U.S. Department of Energy. Computing resources were provided by NYU High Performance Computing, and NCAR's Climate Simulation Laboratory, sponsored by NSF and other agencies. This research was enabled by the computational and storage resources of NCAR's Computational and Information System Laboratory (CISL). We acknowledge support of the US National Science Foundation through grant AGS-1852727 to New York University. M. Linz acknowledges support from NASA New Investigator Program Award 80NSSC21K0943. J. Curbelo also acknowledges the support of the U.S. NSF Grant AGS-1832842 and the RyC project RYC2018-025169. Data availability: FV3 model data available on NYU high performance computing cluster Greene and WACCM model data available on NCAR's supercomputing storage. Zonal mean model data, in a polished form, is being prepared and will be made pubicly available for peer review latest by 15 September 2022.

References

Abalos, M., & de la Cámara, A. (2020). Twenty-First Century Trends in Mixing Barriers and Eddy Transport in the Lower Stratosphere. *Geophysical Research Letters*, *47*(21), e2020GL089548. doi: 10.1029/2020GL089548

Abalos, M., Legras, B., & Shuckburgh, E. (2016). Interannual variability in effective diffusivity in the upper troposphere/lower stratosphere from reanalysis data. *Quarterly Journal of the Royal Meteorological Society*, *142*(697), 1847–1861. doi: 10.1002/qj.2779

Allen, D. R., & Nakamura, N. (2001). A seasonal climatology of effective diffusivity in the stratosphere. *Journal of Geophysical Research: Atmospheres*, *106*(D8), 7917–7935. doi: 10.1029/2000JD900717

Boering, K. A., Wofsy, S. C., Daube, B. C., Schneider, H. R., Loewenstein, M., Podolske, J. R., & Conway, T. J. (1996). Stratospheric Mean Ages and Transport Rates from Observations of Carbon Dioxide and Nitrous Oxide. *Science*.

Chabrillat, S., Vigouroux, C., Christophe, Y., Engel, A., Errera, Q., Minganti, D., ... Mahieu, E. (2018, October). Comparison of mean age of air in five reanalyses using the BASCOE transport model. *Atmospheric Chemistry and Physics*,

18. doi: 10.5194/acp-18-14715-2018

Charney, J. G., & Drazin, P. G. (1961). Propagation of planetary-scale disturbances from the lower into the upper atmosphere. *Journal of Geophysical Research (1896-1977)*, *66*(1), 83–109. doi: 10.1029/JZ066i001p00083

Chen, G., & Plumb, A. (2014, September). Effective Isentropic Diffusivity of Tropospheric Transport. *Journal of the Atmospheric Sciences*, *71*(9), 3499–3520. doi: 10.1175/JAS-D-13-0333.1

Curbelo, J., Chen, G., & Mechoso, C. R. (2021). Lagrangian Analysis of the Northern Stratospheric Polar Vortex Split in April 2020. *Geophysical Research Letters*, *48*(16), e2021GL093874. doi: 10.1029/2021GL093874

Donner, L. J., Wyman, B. L., Hemler, R. S., Horowitz, L. W., Ming, Y., Zhao, M., ... Zeng, F. (2011, July). The Dynamical Core, Physical Parameterizations, and Basic Simulation Characteristics of the Atmospheric Component AM3 of the GFDL Global Coupled Model CM3. *Journal of Climate*, *24*(13), 3484–3519. doi: 10.1175/2011JCLI3955.1

Garcia, R. R., Randel, W. J., & Kinnison, D. E. (2011, January). On the Determination of Age of Air Trends from Atmospheric Trace Species. *Journal of the Atmospheric Sciences*, *68*(1), 139–154. doi: 10.1175/2010JAS3527.1

Garcia, R. R., Smith, A. K., Kinnison, D. E., de la Cámara, Á., & Murphy, D. J. (2017, January). Modification of the Gravity Wave Parameterization in the Whole Atmosphere Community Climate Model: Motivation and Results. *Journal of the Atmospheric Sciences*, *74*(1), 275–291. doi: 10.1175/JAS-D-16-0104.1

Garny, H., Birner, T., Bönisch, H., & Bunzel, F. (2014). The effects of mixing on age of air. *Journal of Geophysical Research: Atmospheres*, *119*(12), 7015–7034. doi: 10.1002/2013JD021417

Garny, H., & Randel, W. J. (2016, March). Transport pathways from the Asian monsoon anticyclone to the stratosphere. *Atmospheric Chemistry and Physics*, *16*(4), 2703–2718. doi: 10.5194/acp-16-2703-2016

Gerber, E. P. (2012, April). Stratospheric versus Tropospheric Control of the Strength and Structure of the Brewer–Dobson Circulation. *Journal of the Atmospheric Sciences*, *69*(9), 2857–2877. doi: 10.1175/JAS-D-11-0341.1

Gupta, A., Gerber, E. P., & Lauritzen, P. H. (2020). Numerical impacts on tracer

transport: A proposed intercomparison test of Atmospheric General Circulation Models. *Quarterly Journal of the Royal Meteorological Society*, *146*(733), 3937–3964. doi: 10.1002/qj.3881

Gupta, A., Gerber, E. P., Plumb, R. A., & Lauritzen, P. H. (2021, September). Numerical impacts on tracer transport: Diagnosing the influence of dynamical core formulation and resolution on stratospheric transport. *Journal of the Atmospheric Sciences*, *-1*(aop). doi: 10.1175/JAS-D-21-0085.1

Hall, T. M., & Plumb, R. A. (1994). Age as a diagnostic of stratospheric transport. *Journal of Geophysical Research*, *99*(D1), 1059. doi: 10.1029/93JD03192

Hall, T. M., Waugh, D. W., Boering, K. A., & Plumb, R. A. (1999). Evaluation of transport in stratospheric models. *Journal of Geophysical Research: Atmospheres*, *104*(D15), 18815–18839. doi: 10.1029/1999JD900226

Held, I. M., & Suarez, M. J. (1994, October). A Proposal for the Intercomparison of the Dynamical Cores of Atmospheric General Circulation Models. *Bulletin of the American Meteorological Society*, *75*(10), 1825–1830. doi: 10.1175/1520-0477(1994)075⟨1825:APFTIO⟩2.0.CO;2

Holton, J. R., Haynes, P. H., McIntyre, M. E., Douglass, A. R., Rood, R. B., & Pfister, L. (1995). Stratosphere-troposphere exchange. *Reviews of Geophysics*, *33*(4), 403–439. doi: 10.1029/95RG02097

Konopka, P., Grooß, J.-U., Plöger, F., & Müller, R. (2009). Annual cycle of horizontal in-mixing into the lower tropical stratosphere. *Journal of Geophysical Research: Atmospheres*, *114*(D19). doi: 10.1029/2009JD011955

Lee, A. M., Roscoe, H. K., Jones, A. E., Haynes, P. H., Shuckburgh, E. F., Morrey, M. W., & Pumphrey, H. C. (2001). The impact of the mixing properties within the Antarctic stratospheric vortex on ozone loss in spring. *Journal of Geophysical Research: Atmospheres*, *106*(D3), 3203–3211. doi: 10.1029/2000JD900398

Lin, S.-J. (2004, October). A "Vertically Lagrangian" Finite-Volume Dynamical Core for Global Models. *Monthly Weather Review*, *132*(10), 2293–2307. doi: 10.1175/1520-0493(2004)132⟨2293:AVLFDC⟩2.0.CO;2

Linz, M., Plumb, R. A., Gerber, E. P., Haenel, F. J., Stiller, G., Kinnison, D. E., ... Neu, J. L. (2017, September). The strength of the meridional overturning circulation of the stratosphere. *Nature Geoscience*, *10*(9), 663–667. doi:

10.1038/ngeo3013

Linz, M., Plumb, R. A., Gerber, E. P., & Sheshadri, A. (2016, August). The Relationship between Age of Air and the Diabatic Circulation of the Stratosphere. *Journal of the Atmospheric Sciences*, *73*(11), 4507–4518. doi: 10.1175/JAS-D-16-0125.1

Linz, M., Plumb, R. A., Gupta, A., & Gerber, E. P. (2021, September). Stratospheric adiabatic mixing rates derived from the vertical gradient of age of air. *Journal of Geophysical Research: Atmospheres*. doi: 10.1029/2021JD035199

Mahlman, J. D., Levy II, H., & Moxim, W. J. (1986). Three-dimensional simulations of stratospheric n2o: Predictions for other trace constituents. *Journal of Geophysical Research: Atmospheres*, *91*(D2), 2687-2707. Retrieved from `https://agupubs.onlinelibrary.wiley.com/doi/abs/10.1029/JD091iD02p02687` doi: https://doi.org/10.1029/JD091iD02p02687

Marsh, D. R., Mills, M. J., Kinnison, D. E., Lamarque, J.-F., Calvo, N., & Polvani, L. M. (2013, October). Climate Change from 1850 to 2005 Simulated in CESM1(WACCM). *Journal of Climate*, *26*(19), 7372–7391. doi: 10.1175/JCLI-D-12-00558.1

Morgenstern, O., Hegglin, M. I., Rozanov, E., O'Connor, F. M., Abraham, N. L., Akiyoshi, H., ... Zeng, G. (2017, February). Review of the global models used within phase 1 of the Chemistry–Climate Model Initiative (CCMI). *Geoscientific Model Development*, *10*(2), 639–671. doi: 10.5194/gmd-10-639-2017

Nakamura, N. (1996, June). Two-Dimensional Mixing, Edge Formation, and Permeability Diagnosed in an Area Coordinate. *Journal of the Atmospheric Sciences*, *53*(11), 1524–1537. doi: 10.1175/1520-0469(1996)053⟨1524:TDMEFA⟩2.0.CO;2

Nakamura, N. (2001, December). A New Look at Eddy Diffusivity as a Mixing Diagnostic. *Journal of the Atmospheric Sciences*, *58*(24), 3685–3701. doi: 10.1175/1520-0469(2001)058⟨3685:ANLAED⟩2.0.CO;2

Neale, R. B., Richter, J., Park, S., Lauritzen, P. H., Vavrus, S. J., Rasch, P. J., & Zhang, M. (2013, July). The Mean Climate of the Community Atmosphere Model (CAM4) in Forced SST and Fully Coupled Experiments. *Journal of Climate*, *26*(14), 5150–5168. doi: 10.1175/JCLI-D-12-00236.1

Neu, J. L., & Plumb, R. A. (1999). Age of air in a "leaky pipe" model of strato-

spheric transport. *Journal of Geophysical Research: Atmospheres*, *104*(D16), 19243–19255. doi: 10.1029/1999JD900251

Neu, J. L., Sparling, L. C., & Plumb, R. A. (2003). Variability of the subtropical "edges" in the stratosphere. *Journal of Geophysical Research: Atmospheres*, *108*(D15). doi: 10.1029/2002JD002706

Pauluis, O., Czaja, A., & Korty, R. (2009, December). The Global Atmospheric Circulation in Moist Isentropic Coordinates. *Journal of Climate*, *23*(11), 3077–3093. doi: 10.1175/2009JCLI2789.1

Ploeger, F., Konopka, P., Müller, R., Fueglistaler, S., Schmidt, T., Manners, J. C., ... Riese, M. (2012). Horizontal transport affecting trace gas seasonality in the Tropical Tropopause Layer (TTL). *Journal of Geophysical Research: Atmospheres*, *117*(D9). doi: 10.1029/2011JD017267

Ploeger, F., Legras, B., Charlesworth, E., Yan, X., Diallo, M., Konopka, P., ... Riese, M. (2019, May). How robust are stratospheric age of air trends from different reanalyses? *Atmospheric Chemistry and Physics*, *19*(9), 6085–6105. doi: 10.5194/acp-19-6085-2019

Ploeger, F., Riese, M., Haenel, F., Konopka, P., Müller, R., & Stiller, G. (2015). Variability of stratospheric mean age of air and of the local effects of residual circulation and eddy mixing. *Journal of Geophysical Research: Atmospheres*, *120*(2), 716–733. doi: 10.1002/2014JD022468

Plumb, R. A. (1996). A "tropical pipe" model of stratospheric transport. *Journal of Geophysical Research: Atmospheres*, *101*(D2), 3957–3972. doi: 10.1029/95JD03002

Plumb, R. A. (2002). Stratospheric Transport. *Journal of the Meteorological Society of Japan. Ser. II*, *80*(4B), 793–809. doi: 10.2151/jmsj.80.793

Plumb, R. A. (2007). Tracer interrelationships in the stratosphere. *Reviews of Geophysics*, *45*(4). doi: 10.1029/2005RG000179

Plumb, R. A., & Ko, M. K. W. (1992). Interrelationships between mixing ratios of long-lived stratospheric constituents. *Journal of Geophysical Research: Atmospheres*, *97*(D9), 10145–10156. doi: 10.1029/92JD00450

Plumb, R. A., & Mahlman, J. D. (1987, January). The Zonally Averaged Transport Characteristics of the GFDL General Circulation/Transport Model. *Journal of the Atmospheric Sciences*, *44*(2), 298–327. doi: 10.1175/1520-0469(1987)

044⟨0298:TZATCO⟩2.0.CO;2

Polvani, L. M., & Kushner, P. J. (2002). Tropospheric response to stratospheric perturbations in a relatively simple general circulation model. *Geophysical Research Letters*, *29*(7), 18-1-18-4. doi: 10.1029/2001GL014284

Putman, W. M., & Lin, S.-J. (2007, November). Finite-volume transport on various cubed-sphere grids. *Journal of Computational Physics*, *227*(1), 55–78. doi: 10.1016/j.jcp.2007.07.022

Ray, E. A., Moore, F. L., Rosenlof, K. H., Davis, S. M., Boenisch, H., Morgenstern, O., ... Plummer, D. A. (2010). Evidence for changes in stratospheric transport and mixing over the past three decades based on multiple data sets and tropical leaky pipe analysis. *Journal of Geophysical Research: Atmospheres*, *115*(D21). doi: 10.1029/2010JD014206

Ray, E. A., Moore, F. L., Rosenlof, K. H., Plummer, D. A., Kolonjari, F., & Walker, K. A. (2016). An idealized stratospheric model useful for understanding differences between long-lived trace gas measurements and global chemistry-climate model output. *Journal of Geophysical Research: Atmospheres*, *121*(10), 5356–5367. doi: 10.1002/2015JD024447

Schneider, T. (2004, June). The Tropopause and the Thermal Stratification in the Extratropics of a Dry Atmosphere. *Journal of the Atmospheric Sciences*, *61*(12), 1317–1340. doi: 10.1175/1520-0469(2004)061⟨1317:TTATTS⟩2.0.CO;2

Shah, K. S., Solomon, S., Thompson, D. W. J., & Kinnison, D. E. (2020). Evaluating Stratospheric Tropical Width Using Tracer Concentrations. *Journal of Geophysical Research: Atmospheres*, *125*(21), e2020JD033081. doi: 10.1029/2020JD033081

Shuckburgh, E., d'Ovidio, F., & Legras, B. (2009, December). Local Mixing Events in the Upper Troposphere and Lower Stratosphere. Part II: Seasonal and Interannual Variability. *Journal of the Atmospheric Sciences*, *66*(12), 3695–3706. doi: 10.1175/2009JAS2983.1

Shuckburgh, E., Norton, W., Iwi, A., & Haynes, P. (2001). Influence of the quasi-biennial oscillation on isentropic transport and mixing in the tropics and subtropics. *Journal of Geophysical Research: Atmospheres*, *106*(D13), 14327–14337. doi: 10.1029/2000JD900664

Waugh, D., & Hall, T. (2002). Age of Stratospheric Air: Theory, Observations, and

Models. *Reviews of Geophysics*, *40*(4), 1-1-1-26. doi: 10.1029/2000RG000101

Yamada, R., & Pauluis, O. (2015, December). Momentum Balance and Eliassen–Palm Flux on Moist Isentropic Surfaces. *Journal of the Atmospheric Sciences*, *73*(3), 1293–1314. doi: 10.1175/JAS-D-15-0229.1

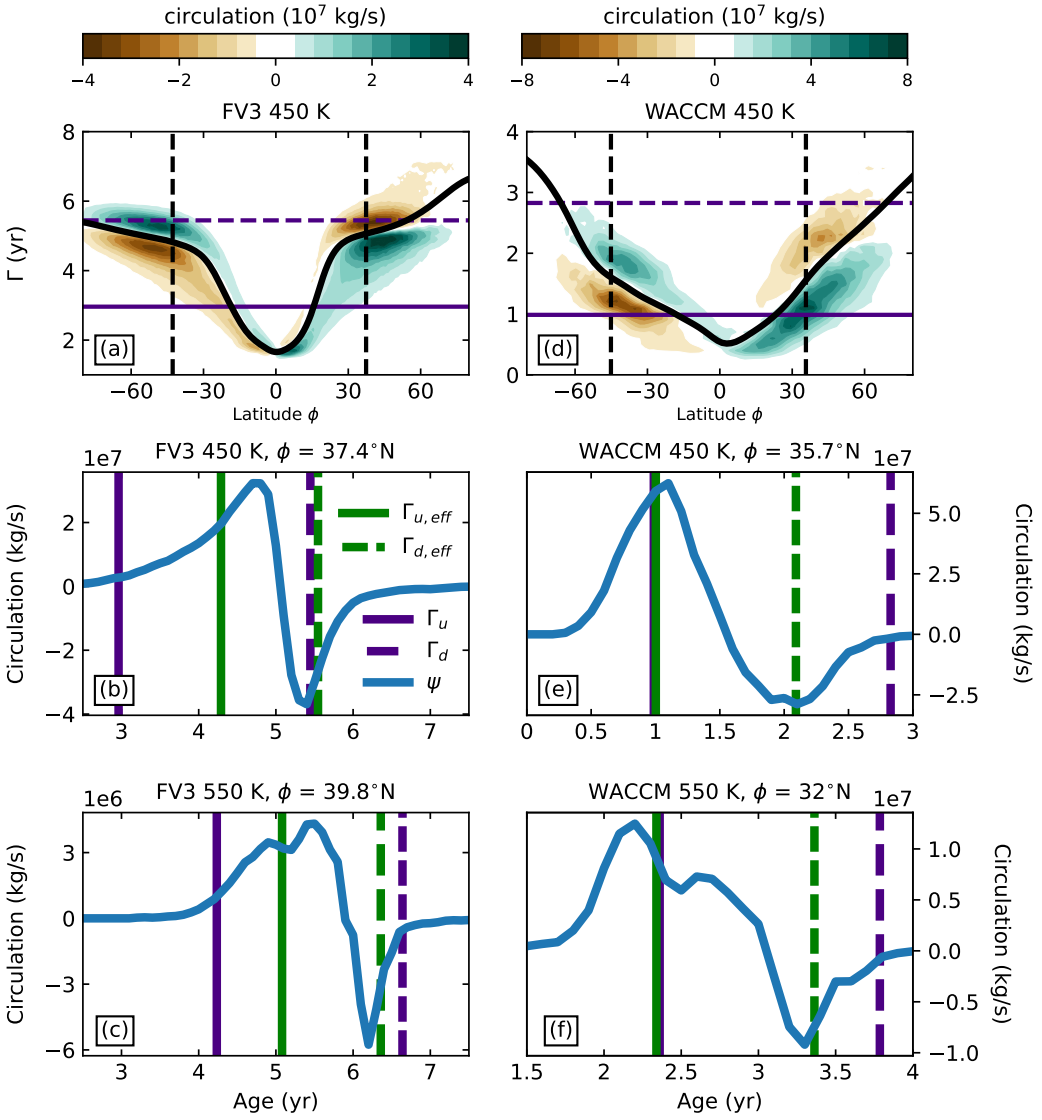

Figure 5. The Γ-θ circulation, ψ, as defined in Equation 4 for (a) the FV3 core and (d) the WACCM model, at 450 K isentropic height. In both (a) and (b), the black curves shows the mean age-of-air at 450 K, and the solid and dashed red lines respectively mark the upwelling and downwelling ages, Γ_u and Γ_d at this height. The dashed black curves in each hemisphere mark the turnaround latitudes at 450 K. Subplots (b) and (e) show a slice of ψ at 450 K in bold blue across a fixed latitude (chosen near the turnaround latitude for FV3 and WACCM respectively, i.e., they show a cross-section of ψ along the dashed black curve in (a) and (d)). Subplots (c) and (f) are identical to subplots (b) and (e) except that they show the distribution on 550 K. In subplots (b-c,e-f), the solid and dashed red vertical bars show Γ_u and Γ_d respectively, while the solid and dashed green vertical bars show the ages $\Gamma_{u,eff}$ and $\Gamma_{d,eff}$ which are calculated from the Γ-θ circulation by a circulation-weighted average over the positive and negative portion of ψ (in blue). The ages $\Gamma_{u,eff}$ and $\Gamma_{d,eff}$ more accurately reflect the ages of the parcels actually being mixed at the given height and indicate an overestimation of the age difference $\Delta\Gamma$ being mixed across the transport barrier, as considered in Equation 2.

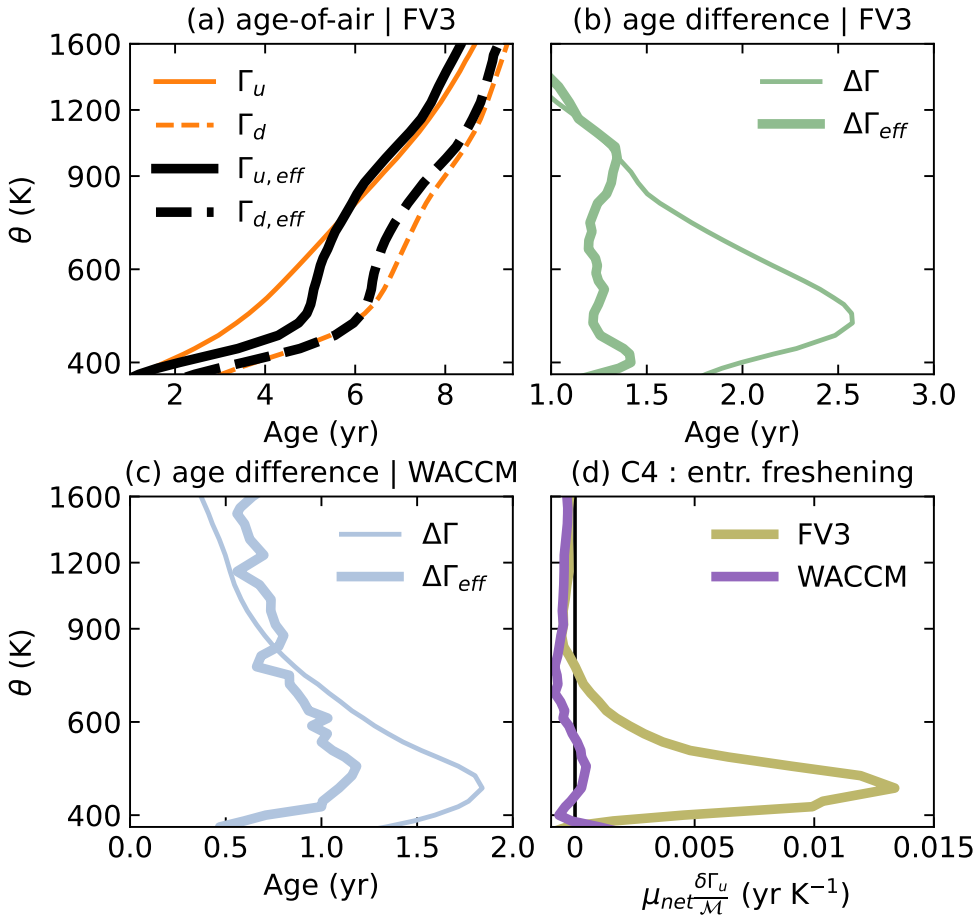

Figure 6. A comparison of the terms between the original mixing equation, Equation 2, and the revised mixing equation, Equation 3. (a) The mass-flux weighted ages Γ_u and Γ_d (in orange) and the $\psi-$weighted ages $\Gamma_{u,eff}$ and $\Gamma_{d,eff}$ (in black) for the idealized FV3 model. The upwelling and downwelling ages are shown using solid and dashed curves respectively. (b) The age differences $\Delta\Gamma$ (thin green) and $\Delta\Gamma_{eff}$ (bold green) as inferred from the ages in subplot (a) for FV3. (c) Corresponding age differences $\Delta\Gamma$ (thin blue) and $\Delta\Gamma_{eff}$ (bold blue) obtained for NDJFM months in WACCM. (d) The entrainment freshening term, i.e., term C4 in Equation 3 for both the idealized FV3 model (yellow) and the comprehensive model WACCM (violet).

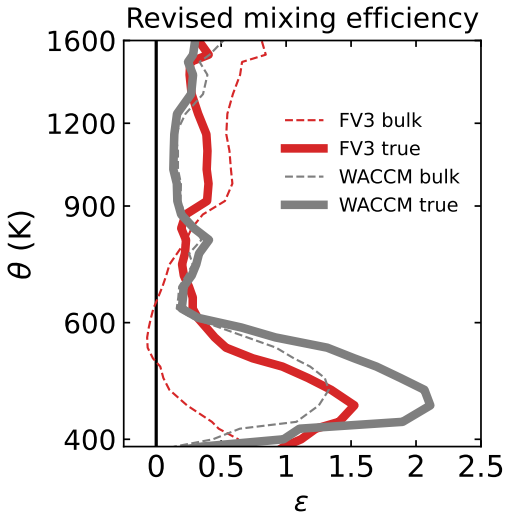

Figure 7. The bulk mixing efficiency and true mixing efficiency ϵ, which are defined as the ratio of the bulk/true mixing flux to the net poleward flux, i.e., bulk $\epsilon = \mu_{mix}/\mu_{net}$ and true $\epsilon = \mu^T_{mix}/\mu_{net}$. The mixing efficiency obtained by applying Equation 3 is shown using thick solid curves. The mixing efficiency obtained for both FV3 (red) and WACCM (grey) using the original mixing equation of Linz et al. (2021) is shown using thin dashed curves for reference.

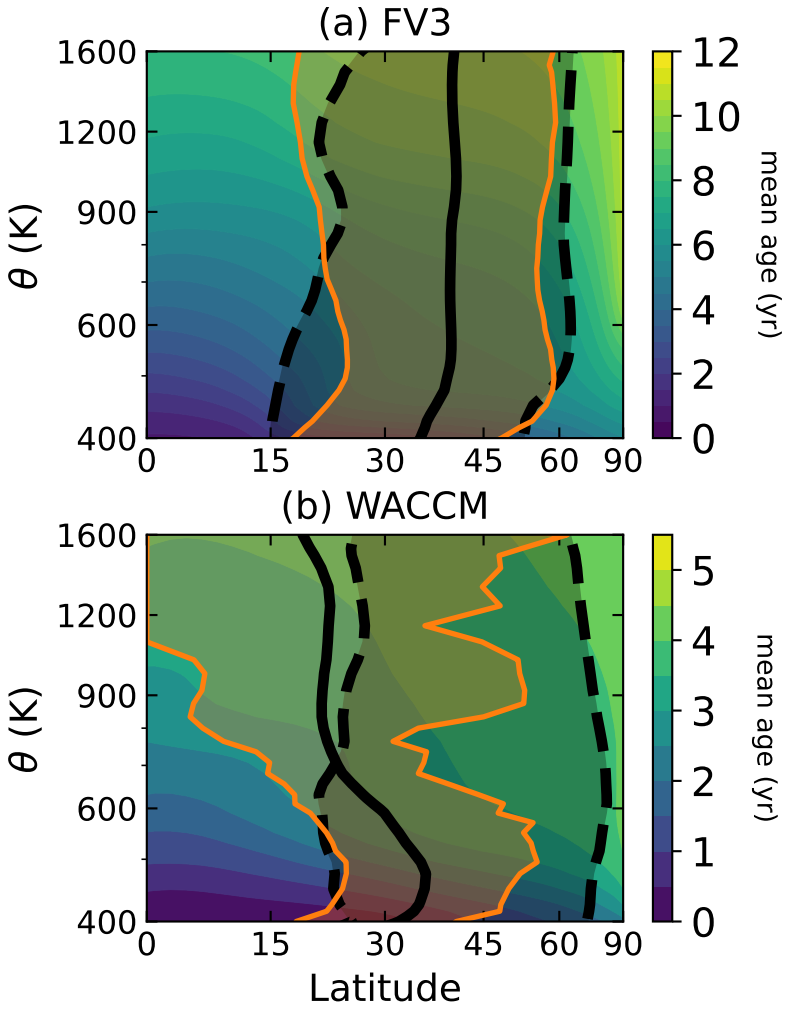

Figure 8. Age inferred meridional range of adiabatic mixing in (a) the idealized FV3 core and (b) the comprehensive model WACCM. For both the plots, the zonal mean age profile is shown in color. The solid black curve shows the turnaround latitude, and the dashed black curves on either side show the latitudes with Γ_u and Γ_d as the mean age. The orange curves, and the area enclosed, demarcate the extent of the mixing region inferred from the mean ages $\Gamma_{u,eff}$ and $\Gamma_{d,eff}$. These ages were estimated as an average of the circulation distribution around the turnaround latitude. The analysis reveals little-to-no mixing of the midlatitude air into the deep tropics. The deep tropics are markedly more isolated for the FV3 core, than for the WACCM model. Both the subplots use separate colorbars.